Published online 23 March 2022

Nucleic Acids Research, 2022, Vol. 50, No. 7 ***3745–3763***
https://doi.org/10.1093/nar/gkac178

Nuclear receptor activation shapes spatial genome organization essential for gene expression control: lessons learned from the vitamin D receptor

Timothy Warwick[1,3], Marcel H. Schulz[2,3], Ralf Gilsbach[1,3], Ralf P. Brandes[1,3] and Sabine Seuter[1,3,*]

[1]Institute for Cardiovascular Physiology, Goethe University, Frankfurt/Main, Germany, [2]Institute for Cardiovascular Regeneration, Goethe University, Frankfurt/Main, Germany and [3]German Center for Cardiovascular Research (DZHK), Partner site Rhein-Main 60590, Frankfurt am Main, Germany

Received August 09, 2021; Revised February 23, 2022; Editorial Decision March 04, 2022; Accepted March 07, 2022

ABSTRACT

Spatial genome organization is tightly controlled by several regulatory mechanisms and is essential for gene expression control. Nuclear receptors are ligand-activated transcription factors that modulate physiological and pathophysiological processes and are primary pharmacological targets. DNA binding of the important loop-forming insulator protein CCCTC-binding factor (CTCF) was modulated by 1α,25-dihydroxyvitamin D_3 (1,25$(OH)_2D_3$). We performed CTCF HiChIP assays to produce the first genome-wide dataset of CTCF long-range interactions in 1,25$(OH)_2D_3$-treated cells, and to determine whether dynamic changes of spatial chromatin interactions are essential for fine-tuning of nuclear receptor signaling. We detected changes in 3D chromatin organization upon vitamin D receptor (VDR) activation at 3.1% of all observed CTCF interactions. VDR binding was enriched at both differential loop anchors and within differential loops. Differential loops were observed in several putative functional roles including TAD border formation, promoter-enhancer looping, and establishment of VDR-responsive insulated neighborhoods. Vitamin D target genes were enriched in differential loops and at their anchors. Secondary vitamin D effects related to dynamic chromatin domain changes were linked to location of downstream transcription factors in differential loops. CRISPR interference and loop anchor deletion experiments confirmed the functional relevance of nuclear receptor ligand-induced adjustments of the chromatin 3D structure for gene expression regulation.

INTRODUCTION

In genome architecture, chromosome territories followed by active A and inactive B compartments represent the highest hierarchy of organization (1,2). The next scale of 3D chromatin domains contains topologically associating domains (TADs, ∼1 Mb), which are characterized by a high degree of self-interaction (1,3,4). Structures identified in the sub-TAD range have been termed insulated neighborhoods, contact domains or loop-domains (5,6).

The zinc finger transcription factor and insulator protein CTCF binds at TAD boundaries and has been proposed to form loops together with cohesin by loop extrusion (1,3,7–14). Insulators can block the spread of active or repressive chromatin (15,16), or protect a gene from ectopic activation if located between the gene and an enhancer (17). Also, the interaction of two insulators with each other by chromatin looping can bring an enhancer in proximity to a promoter or, contrastingly, tether it to a locus away from a promoter (18,19).

The impact of TADs in enhancer function and gene regulation is diverse (20). CTCF has been proposed to maintain a nucleosome-free, accessible region at promoters (21). The observed effects of TAD boundary deletion on gene expression ranged from no functional impact to severe effects (16,22–34). Consequences of chromatin rearrangements include TAD fusions, enhancer hijacking, ectopic enhancer-promoter loops, and insertions of new CTCF boundaries, all of which may lead to changes in gene expression (22–24,32–40).

Intra-TAD interactions are frequent and it has been suggested that a TAD facilitates contacts between enhancers and promoters inside the TAD. The restriction of absolute 3D distance may help to obtain robust and precise transcription, partly by establishing a high local concentration of transcription factors (20).

The CTCF cistrome and the CTCF-mediated long-range interactions are highly conserved across human, mam-

*To whom correspondence should be addressed. Tel: +49 69 6301 6996, Email: seuter@vrc.uni-frankfurt.de

malian and vertebrate cell types, as shown by chromatin immunoprecipitation sequencing (ChIP-seq), 'Chromatin Interaction Analysis by Paired-end tag Sequencing' (ChIA-PET) and Hi-C experiments in different cellular systems in their basal state (3,41–50). However, gene expression changes during cellular differentiation and senescence have been linked to rearrangements in loops and compartments (51–53). In addition, a subset of heat shock-upregulated genes displayed a modestly increased frequency of chromatin interactions (54). Depletion of CTCF or cohesin in cell culture in a steady state dramatically perturbed TAD formation leading to differential expression of hundreds of genes (11–14,55–59). The resulting expression changes were moderate, though. Thus, it was concluded that chromatin topology is not essential for enhancer-promoter interactions. A more complex role of 3D chromatin architecture on transcriptional regulation can be assumed that needs to be elucidated in non-steady state models as development, differentiation or cell signaling (60).

The nuclear receptor superfamily is a large group of ligand-activated transcription factors, reviewed in (61–64). They have a wide variety of essential functions in processes such as cell signaling, survival, or proliferation.

The VDR is a classical endocrine receptor and belongs to the retinoid X receptor (RXR) heterodimer-forming class II nuclear receptors. It is activated by its high affinity ligand $1,25(OH)_2D_3$, the most active metabolite of vitamin D_3. VDR preferentially binds as a heterodimer with RXR to DR3-type response elements, which are formed by a direct repeat of two hexameric sequence motifs spaced by three nucleotides (65,66). A prerequisite of VDR DNA binding is the location of the binding site in accessible chromatin, which can be achieved by the action of pioneer factors like purine-rich box 1 (PU.1) and CCAAT/enhancer binding protein alpha (CEBPA) (67,68). Ligand-bound VDR interferes with chromatin modifiers (69–71), leading to an increase of active histone marks and open chromatin (72,73).

There are some reports on interference of nuclear receptors with 3D chromatin structure, often only investigating individual genomic loci. Examples include links between thyroid hormone receptor (TR) stimulation and CTCF enhancer blocking (74,75), chromatin remodelling at the *HOXA* locus upon stimulation of retinoic acid receptor (RAR) α, β and γ (76), and the interplay between CTCF and ER loop formation in breast cancer cells (77). In the latter case, mechanisms including 3D epigenome remodelling have been proposed to influence endocrine resistance in ER+ breast cancer (78).

As $1,25(OH)_2D_3$ modulated the binding of CTCF in roughly 2,100 genomic regions in monocytic THP-1 cells (73,79), we hypothesized that it thereby may modulate the CTCF-defined chromatin structure. So far, no genome-wide studies investigated chromatin interactions upon $1,25(OH)_2D_3$ treatment of cells or VDR-related interactions. Thus, in this study we performed CTCF HiChIP assays to identify $1,25(OH)_2D_3$-induced rearrangements in chromatin topology. We found that the frequency of >3,000 CTCF interactions was changed by the VDR ligand. VDR binding sites and vitamin D target genes were enriched inside these differential loops and often located at the loop anchors. In addition, transcription factors encoded by primary vitamin D target genes were enriched in the differential loops. Clustered regularly interspaced short palindromic repeats interference (CRISPRi) experiments validated a VDR co-bound CTCF loop anchor as functional enhancer of the prostaglandin E synthase 2 (*PTGES2*) gene. Deletion of anchors of differential loops resulted in modulated vitamin D regulation of some genes inside and neighboring the loops. Thus, the physiological stimulus with the nuclear receptor ligand $1,25(OH)_2D_3$ induced functionally important changes in the 3D chromatin architecture in living cells.

MATERIALS AND METHODS

Cell culture

The human acute monocytic leukemia cell line THP-1 is a well responding and physiologically meaningful model system for the investigation of $1,25(OH)_2D_3$-triggered physiological processes, such as innate immunity and cellular growth. The cells were grown in RPMI 1640 medium, supplemented with 10% fetal calf serum (FCS), 2 mM L-glutamine, 0.1 mg/ml streptomycin and 100 U/ml penicillin, and were kept at 37°C in a humidified 95% air/5% CO_2 incubator. Prior to experiments, cells were grown overnight in phenol red-free medium supplemented with charcoal-stripped FCS and then treated with vehicle (0.1% ethanol (EtOH)) or 100 nM $1,25(OH)_2D_3$ (Sigma-Aldrich) for 24 h.

Lenti-X 293T cells (Takara Bio) were grown in DMEM medium supplemented with 10% FCS, 0.1 mg/ml streptomycin and 100 U/ml penicillin and were kept at 37°C in a humidified 95% air/5% CO_2 incubator.

CTCF HiChIP

HiChIP assays of three biological repeats were performed as described by Mumbach *et al.* (80), with some modifications. After treatment of 30×10^6 THP-1 cells, nuclear proteins were cross-linked to genomic DNA by adding formaldehyde directly to the medium to a final concentration of 1% and incubating at room temperature for 10 min on a rocking platform. Cross-linking was stopped by adding glycine to a final concentration of 0.125 M and incubating at room temperature for 10 min on a rocking platform. The cells were collected by centrifugation and washed twice with ice cold phosphate-buffered saline (PBS). Cells were lysed in 1 ml Hi-C Lysis Buffer (10 mM Tris–HCl pH 8.0, 10 mM NaCl, 0.2% NP-40, protease inhibitors) with rotation at 4°C for 30 min and split into two aliquots. Nuclei were washed with Hi-C Lysis Buffer and incubated with 100 µl 0.5% SDS at 62°C for 10 min. SDS was quenched with 285 µl H_2O and 50 µl 10% Triton X-100 rotating at 37°C for 15 min. Restriction digestion with 15 µl *MboI* (New England Biolabs) in NEB Buffer 2.1 was performed rotating at 37°C for 2 h. The pellet was washed twice with and resuspended in NEB Buffer 2.1. Overhangs were filled in and marked with biotin by adding 37.5 µl 0.4 mM Biotin-14-dATP (Thermo Fisher Scientific), 1.5 µl 10 mM dCTP, 1.5 µl 10 mM dGTP, 1.5 µl 10 mM dTTP and 5 µl 10 U/µl DNA Polymerase I,

Large (Klenow) Fragment (Thermo Fisher Scientific) and rotating at 37°C for 1 h. Then, proximity ligation was performed by 4 h rotation after addition of 150 μl 10× NEB T4 DNA ligase buffer with 10 mM ATP (Thermo Fisher Scientific), 125 μl 10% Triton X-100, 3 μl 50 mg/ml BSA, 4 μl 1000 CEU/μl T4 DNA Ligase (Thermo Fisher Scientific), and 666 μl H_2O. The supernatant was removed by centrifugation and nuclei were resuspended in 500 μl SDS lysis buffer (50 mM Tris–HCl pH 8.1, 10 mM EDTA, 1% SDS, protease inhibitors). The two aliquots were recombined and sonicated in a Bioruptor Plus (Diagenode) for 5 min. Then, debris was removed. Chromatin Immunoprecipitation was performed by adding 400 μl chromatin aliquots and 1600 μl IP Dilution Buffer (20 mM Tris–HCl pH 7.5, 2 mM EDTA, 1% Triton X-100, 150 mM NaCl, protease inhibitors) to each 90 μl Dynabeads Protein G (Invitrogen), pre-coupled with 4 μl CTCF antibody (Millipore 07–729), and rotating at 4°C for over night. The next day, the beads were washed 3× with Cell Lysis Buffer (50 mM HEPES–KOH pH 7.5, 1 mM EDTA, 1% Triton X-100, 150 mM NaCl, 0.1% SDS, 0.1% sodium deoxycholate, protease inhibitors), 1× with High Salt Buffer (50 mM HEPES–KOH pH 7.5, 1 mM EDTA, 1% Triton X-100, 350 mM NaCl, 0.1% SDS, 0.1% sodium deoxycholate, protease inhibitors), 1× with ChIP Wash Buffer (10 mM Tris–HCl pH 8.0, 1 mM EDTA, 0.5% NP-40, 250 mM LiCl, 0.5% sodium deoxycholate, protease inhibitors) and 2× with TE Buffer. Two sequential elutions were carried out with 150 μl DNA Elution Buffer (50 mM $NaHCO_3$, 1% SDS) (10 min room temperature, 3 min 37°C) and both eluates from all replicate IPs were pooled. Proteins were digested with Proteinase K and crosslinks were reversed for 2 h at 65°C, followed by DNA purification with the ChIP DNA Clean & Concentrator kit (Zymo Research). Biotin capture was performed with 5 μl washed Dynabeads MyOne Streptavidin C1 (Invitrogen) for 15 min at room temperature. Beads were washed with Tween Wash Buffer (5 mM Tris–HCl pH 7.5, 0.5 mM EDTA, 0.05% Tween-20, 1 M NaCl) and 1× Tagmentation Buffer. Tagmentation with Tn5 transposase (Illumina) in a 50 μl reaction using the appropriate amount of Tn5 transposase for every sample as detailed by Mumbach *et al.* (80) and incubating at 55°C for 10 min. The reaction was stopped by addition of EDTA and beads were washed with Tween Wash Buffer and 10 mM Tris pH 7.5. Library preparation and size selection were performed as described in the Mumbach protocol (80). Library quality was controlled by High Sensitivity DNA Assay on an Agilent Bioanalyzer. The sequencing was performed at Novogene (HK) on an Illumina Hiseq-PE150. The sequencing depths obtained per sample were between 300 and 400 million reads.

CTCF HiChIP data analysis

Paired-end tags arising from CTCF HiChIP were preprocessed, aligned to the *hg19* genome, and used to construct iteratively corrected contact maps using *HiC-Pro* (v2.11.1) (81) in combination with MboI restriction fragments generated using the *HiC-Pro* utility script *digest_genome.py*, and otherwise default parameters. Loops were called per replicate using *hichipper* (v0.7.0) (82) with the EACH,ALL parameter set for CTCF peak identification, and otherwise default parameters. Loop counts per sample were subsequently used as input to *diffloop* (v1.20.0) (83) for identification of differential CTCF-mediated chromatin interactions. Only loops with a *mango* (included in *hichipper*) adjusted P value <0.01 were used as input, as per the *diffloop* vignette. Loop counts were considered to be artefacts when a loop count of >5 was observed in one replicate of a treatment group, but not observed at all in an accompanying replicate. Differential analysis was carried out using the *quickAssocVoom* function, thereby using the limma-voom empirical Bayes analysis pipeline used in differential analysis previously in the *limma* and *voom* R packages. Differential interactions were those with an adjusted P value <0.05 (Benjamini–Hochberg correction).

Loops were initially annotated using *hg19* gene coordinates (*RefSeq*), promoters (TSS ± 2500 bp) and regulatory elements (*EpiRegio*) (84). Annotation was performed using the *GenomicInteractions* R package (v1.26.0) to generate a *GenomicInteractions* object from the called loops, and *GenomicFeatures* objects from the aforementioned gene, promoter and regulatory element coordinates, followed by running *annotateInteractions* (85).

In order to compute enrichment of features with respect to differential CTCF HiChIP loops, an identically sized set of shuffled loops was generated, alongside using a randomized set of non-differential CTCF loops. The shuffled loops maintained identical loop anchor sizes and loop spans to the differential loops, and were shuffled randomly throughout the genome using *bedtools* (v2.27.1) (86), avoiding regions of the genome included in the ENCODE blacklist. The non-differential (stable) CTCF HiChIP loops were 1000 sets of randomly sampled loops with a differential P_{adj} >0.9, each with the same number of loops as the differential set. Distances and intersects between features were computed using *bedtools intersect* and *bedtools closest*. Virtual 4C was conducted using the *GENOVA* R package (v1.0.0) (87), in conjunction with background interaction frequency data calculated using the *HiCExplorer* (v3.7.2) *chicViewpointBackgroundModel* tool (88), using all loop anchor regions as reference points to build the model. Intersections were considered to be ≥1 bp overlaps between features, with the exception of TAD borders, which were extended by 25 kb upstream and downstream using *bedtools slop*. Statistically significant distances were ascribed between differential and shuffled loop sets by use of Fisher's Exact Test for count data, or by a Kolmogorov–Smirnov test for cumulative distributions. When comparing the differential loop set against the stable loop sets, the proportion of stable loop sets which exceeded the differential set in each particular metric was taken as the P value. To calculate this, the enrichment of the feature in question was computed for each set of stable loops alongside the differential loop set. Each stable enrichment was then compared to the differential enrichment, and the proportion of stable loop sets where the enrichment exceeded the differential enrichment was used as the resulting P value.

The quality control metrics are displayed in Supplementary Figure S1A.

Hi-C

Hi-C assays were performed in duplicate biological repeats using the Arima-HiC kit following the manufacturer's user guide, with some modifications. Briefly, 2.5×10^6 THP-1 cells were cross-linked with 2% formaldehyde for 10 min, stopped with glycine, washed twice with PBS and snap-frozen. The thawed cells were lysed in 20 μl lysis buffer (15 min 4°C), then incubated with 24 μl Conditioning solution (10 min 62°C) and 20 μl Stop Solution 2 (15 min 37°C). Digestion with 12 μl Enzymes A1/A2 master mix was performed by sequential incubations of 45 min 37°C, 20 min 65°C and 10 min 25°C. Then, the biotin fill-in was performed with 16 μl Enzyme B master mix (45 min RT), followed by proximity ligation with 82 μl Enzyme C master mix (15 min RT). Proteins were digested with 35.5 μl Enzyme D master mix plus 20 μl Buffer E in the sequential incubations of 30 min 55°C, 90 min 68°C and 10 min 25°C. The DNA was purified using 100 μl AMPureXP beads (Beckman Coulter). After passing the QC1 quality control, 5 μg of each sample was diluted to 100 μl with Elution Buffer supplemented by 1% SDS. Fragmentation to an average fragment size of ≈400 bp was done by 15 cycles sonication in a Bioruptor Plus (Diagenode) with 30 s ON, 30 s OFF at high intensity. Size selection was performed with 60 μl and 40 μl SPRIselect beads (Beckman Coulter). Biotin enrichment was performed with 0.9–2 μg of the size selected DNA using 50 μl Enrichment Beads for <1 μg DNA and 100 μl for >1 μg DNA (15 min RT). Following washes with Wash Buffer and Elution Buffer end repair and adapter ligation were performed: incubation with 20 μl Enzyme W2 master mix (10 min 37°C), washes, incubation with 50 μl Enzyme G3/G4 master mix (20 min 20°C), washes, ligation of a uniquely indexed P7 TruSeq LT Adapter (Swift Biosciences Set A Indexing Kit) in 25 μl Enzyme Y1 master mix (15 min 25°C), washes, ligation of non-indexed P5 TruSeq Universal adapter (Swift Biosciences Indexing Kit) in 50 μl Enzyme B4/B5/B6 master mix, washes, resuspension. The sufficient cycle number was determined with an initial PCR using 2 μl of the resuspended beads. The remainder of the beads was subjected to library amplification. Samples, for which 100 μl Enrichment Beads had been used, were distributed into six 50 μl PCR reactions, while those with 50 μl Enrichment Beads were run in three 50 μl reactions. PCRs were performed using the KAPA 2X HiFi HotStart Ready Mix (KAPA Biosystems), KAPA Library Amplification Primer Mix and EvaGreen (BioRad). The replicate PCR reactions were pooled, separated from the beads and purified with AMPureXP beads (Beckman Coulter). Concentrations were measured using the Qubit dsDNA HS Assay Kit (Thermofisher Scientific) and quality-controled by High Sensitivity DNA Assay on an Agilent Bioanalyzer or by D1000 ScreenTape on a TapeStation (Agilent). Sequencing was performed by Dr. Stefan Günther at Max-Planck-Institute for Heart and Lung Research, Bad Nauheim, Germany, on an Illumina NextSeq 500-PE100. The sequencing depths obtained per sample were between 76.2 and 151.3 million reads.

Hi-C data analysis

For the analysis, the duplicates were merged to provide greater sequencing depths. Hi-C sequencing reads were aligned to the *hg19* genome using *Bowtie2* with the *–local* and *–reorder* parameters set. The subsequently generated alignment files were then used to build Hi-C matrices with the *HiCExplorer* (v3.7.2) tool *hicBuildMatrix*. The built matrices were then normalized to the smallest of the samples using *hicNormalise,* and then corrected using iterative correction with *hicCorrectMatrix*, with the parameter *–correctionMethod ICE* and thresholds taken from diagnostic plots created using *hicCorrectMatrix diagnostic_plot*. Corrected matrices were then used in the construction of relevant viewpoints using *chicViewpointBackgroundModel* and *chicViewpoint*. The background model was computed across all identified differential loop anchors in the CTCF HiChIP analysis.

Differential TADs were detected using the *R* package *TADCompare* (1.2.0) (89). This used eigenvector gaps to compare boundaries and subsequently identify dynamic and stable boundaries between conditions. Input matrices of 50 kb resolution were imported into R and then the TADCompare command was used for differential TAD detection.

The quality control metrics are displayed in Supplementary Figure S1B and C.

Transcription factor binding prediction

We used TEPIC 2.2 to predict transcription factor affinity at areas of open chromatin in CTCF loop anchor regions (90). Open chromatin regions were detected with formaldehyde-assisted isolation of regulatory elements sequencing (FAIRE-seq) in THP-1 cells after 24 h of 100 nM $1,25(OH)_2D_3$ treatment (73). Transcription factor binding sites were predicted using position specific energy matrices derived from JASPAR 2020 (91), HOmo sapiens COmprehensive MOdel COllection (HOCOMOCO) (92) and Kellis ENCODE motif databases (93), which are part of the TEPIC 2 repository. Predicted binding of a transcription factor at a loop anchor region was assumed where the predicted transcription factor binding affinity at any FAIRE-seq peak in the loop anchor region was significantly strong. Significance was computed using a background set of regions with similar GC-content and length distribution as the original FAIRE-seq peak set as described in (94). Each TF affinity value that met a TEPIC-computed threshold ($P < 0.05$) was considered significant. Thus, the number of loop anchors where each transcription factor was predicted to bind could be quantified and compared between differential and shuffled loop anchors.

CRISPR/Cas9-mediated loop anchor deletions

Specific gRNAs targeting regions upstream and downstream of the selected CTCF loop anchor sites were designed using the Benchling life sciences R&D cloud (https://www.benchling.com). A combination of two gRNAs was used to obtain a deletion. Sense and antisense oligonu-

cleotides containing the 19 bp gRNA sequence plus the required overhangs matching the *BsmBI*-cut vector were purchased (Sigma-Aldrich) and annealed (Supplementary Table S2). Then, *BsmBI* (*Esp3I*) (Thermo Fisher) and T4 DNA ligase (Thermo Fisher) were used to clone the annealed gRNAs into the plasmid containing expression cassettes for hSpCas9 and the chimeric guide RNA with the Golden Gate assembly protocol (95). The vector used was either LentiCRISPRv2 (Addgene #52961 (96)) conveying puromycin resistance, or a modification thereof including hygromycin resistance. Thus, a combination of two gRNAs cloned in the two different plasmids allowed for double selection after the transduction (Supplementary Table S3). Correct insertions of the gRNAs into the plasmid were verified by Sanger sequencing.

Cell-free, lentiviral supernatants were produced by polyethylenimine (PEI)-based transient co-transfection of Lenti-X 293T cells. Briefly, the pLentiGuide-Puro-gRNA vector, the lentiviral gag/pol packaging plasmid psPAX (Addgene #12260; gift from Didier Trono; http://n2t.net/addgene:12260; RRID:Addgene_12260) and the envelope plasmid encoding the glycoprotein of vesicular stomatitis virus (VSV-G) (pMD2.G, Addgene #12259; gift from Didier Trono; http://n2t.net/addgene:12259; RRID:Addgene_12259) were transfected at a molar ratio of 3:1:1 by standard PEI transfection. 24 and 48 h post-transfection, two consecutive viral supernatants were harvested, cleared through 0.45-μm pore-size PVDF membrane filter (Millipore), combined and stored at −80°C.

The transduction with the gRNA-expressing plasmids was performed in two consecutive spinoculations. Briefly, 0.2×10^6 cells were pelleted and resuspended in 1 ml of the lentiviral particles. Polybrene (8 μg/ml) was added and the cells were centrifuged for 90 min with 1000 × g at room temperature. The supernatant was discarded, the cells resuspended in 1 ml full growth medium and incubated for 48–72 h. Then, the second spinoculation was carried out with 800 μl of lentivirus. After another 48–72 h incubation, puromycin (2 μg/ml) and hygromycin (400 μg/ml) were added to select the transduced cells for 10–14 days.

The successful deletions were confirmed by agarose gel electrophoresis of the amplicons of PCRs with genomic DNA as template (data not shown). In cases, where no complete deletion was obtained in the whole cell population, clonal expansion was performed. Positive single cell clones were then selected for subsequent experiments. RT-qPCR was performed to assess possible changes of the transcriptional response to $1,25(OH)_2D_3$ after the deletion.

The deletion of the right anchor of the second differential loop in the ADAM like decysin 1 (*ADAMDEC1*) locus was very efficient for two different gRNA combinations (L66 and L67), thus the experiments were performed with both whole cell populations without clonal expansion. For all other loop anchor deletions single cell clones were created.

Prior to each experiment for RNA extraction, the CRISPR cells were re-selected with puromycin (2 μg/ml) and hygromycin (400 μg/ml) for 3 days.

CRISPR interference

Specific gRNAs targeting CTCF loop anchor regions, VDR enhancer or transcription start site (TSS) have been designed using the Benchling life sciences R&D cloud (https://www.benchling.com) or the GPP sgRNA Designer (https://portals.broadinstitute.org/gpp/public). Sense and antisense oligonucleotides containing the 19 bp gRNA sequence plus the required overhangs matching the *BsmBI*-cut vector were purchased (Sigma-Aldrich) and annealed (Supplementary Table S4). Then, *BsmBI* (*Esp3I*) (Thermo Fisher) and T4 DNA ligase (Thermo Fisher) were used to clone the annealed gRNAs into the plasmid pLV hU6-sgRNA hUbC-dCas9-KRAB-T2a-GFP (Addgene #71237, gift from Charles Gersbach (97)) containing expression cassettes for the catalytically inactive dCas9 fused to the transcriptional repression domain Krüppel-associated box (KRAB) and the chimeric guide RNA with the Golden Gate assembly protocol (95). Correct insertions of the gRNAs into the plasmid were verified by Sanger sequencing.

Lentivirus preparation and transductions were performed as described above for the CRISPR deletions, with the difference that 0.4×10^6 cells have been used. Four days after the second spinoculation, the cells were seeded in medium containing charcoal-stripped FCS. The next day, cells were treated with $1,25(OH)_2D_3$ or ethanol prior to RNA extraction.

RNA isolation, cDNA synthesis and qPCR

Total RNA was extracted using the RNA Mini Kit (Bio-Sell) according to the manufacturer's instructions. cDNA synthesis was performed using Superscript III reverse transcriptase (Invitrogen) and oligo$(dT)_{23}$ primers according to the manufacturer's instructions. PCR reactions were performed with the AriaMx Real-Time PCR System (Agilent Technologies) using 250 nM of reverse and forward primers, cDNA and the iTaq Universal SYBRGreen Supermix (Bio-Rad). Primer-specific temperatures and sequences are listed in Supplementary Table S1. Relative mRNA expression levels were determined using the formula $2^{-(\Delta Ct)}$, where ΔCt is $Ct_{(target\ gene)}$ − mean $Ct_{(reference\ genes)}$. The genes beta-2-microglobulin (*B2M*), glycerinaldehyde-3-phosphate-dehydrogenase (*GAPDH*) and hypoxanthine phosphoribosyltransferase 1 (*HPRT1*) were used as references as described previously (98).

All RT-qPCR experiments have been performed in at least triplicate biological replicates. One-sample Student's t-tests were performed to determine the significance of changes of mRNA inductions by $1,25(OH)_2D_3$ in reference to solvent-treated cells and to determine the significance of % expression changes compared to NTC control cells. The significance of all other effects was determined by two-tailed Student's *t*-tests (* $P < 0.05$; ** $P < 0.01$; *** $P < 0.001$).

Previously published RNA and chromatin data

VDR ChIP-seq data in THP-1 cells is publicly available at NCBI Gene expression Omnibus (GEO) under the accession GSE89431, originally published by Neme *et al.*

(99). CTCF ChIP-seq data in THP-1 cells is publicly available under the accession GSE69962 (73,79). RNA-seq time course data in THP-1 cells with 2.5 h, 4 h and 24 h of 100 nM $1,25(OH)_2D_3$ treatment is accessible at the accession GSE69303 (73,99). FAIRE-seq data in THP-1 cells after 24 h of 100 nM $1,25(OH)_2D_3$ treatment is available from the same source under the accessions GSE69297 and GSE69303, originally published by Seuter *et al.* (73). ETS1 ChIP-seq data from $1,25(OH)_2D_3$-treated THP-1 cells can be obtained from GEO under GSE157209 (100). Digestion-ligation-only Hi-C (DLO-Hi-C) is available under the accession GSE89663 (101).

The Integrative Genomics Viewer (IGV) browser was used to visualize the genome-wide datasets (102).

RESULTS

$1,25(OH)_2D_3$ treatment modulates functional CTCF-defined chromatin structure in monocytic cells

In this study, we have aimed to decipher dynamic changes in CTCF-mediated long-range chromatin interactions tethered by CTCF in THP-1 cells treated for 24 h with 100 nM $1,25(OH)_2D_3$ using CTCF HiChIP assays (Figure 1A). A replicate-based analysis identified in total 2,408,953 loops across 260,099 anchors present across any replicate. 160,291 interactions were present in every control sample and 190,889 loops in every $1,25(OH)_2D_3$-treated sample (Supplementary Figures S2A and B). Of those, 109,764 were detected in both conditions (Figure 1B).

Differential chromatin topology analysis identified 3,433 loops, whose frequency was significantly changed ($P_{adj} < 0.05$, *diffloop*) by the stimulation. Of these differential loops, 2,480 were more frequently observed in $1,25(OH)_2D_3$-treated cells, and 953 were less frequent in treated cells (Figure 1C). The number of $1,25(OH)_2D_3$-sensitive loops was similar to the number of vitamin D target genes that has been published in THP-1 cells (73,99), slightly higher than the number of $1,25(OH)_2D_3$-modified CTCF ChIP-seq peaks (73,79), but much lower than the number of differential VDR ChIP-seq peaks (99) (Supplementary Figure S2C**).** CTCF ChIP-seq peaks were also reproduced in CTCF HiChIP, with ∼84% of ChIP-seq peaks also being called in HiChIP data (Supplementary Figures S2D and E), although the crossover between differential CTCF ChIP-seq peaks and differential loop anchors was not extensive (Supplementary Figure S2F). We found that the differential loops were enriched for putative promoter-promoter, promoter-enhancer and enhancer-enhancer interactions (Figure 1D, Supplementary figures S3A and B). Notably, a higher ratio of $1,25(OH)_2D_3$-upregulated loops (30.5%) was classified as putative promoter-enhancer loops compared to downregulated loops (23.6%) ($P < 0.0001$, Fisher's exact test) (Figure 1D, Supplementary figures S3C and D).

Virtual 4C viewpoint analyses visually confirmed for a number of loci the differential chromatin interactions identified by the replicate-based analysis. A representative differential loop encapsulates the differentially expressed gene (DEG) potassium channel tetramerization domain containing 12 (*KCTD12*), along with several VDR ChIP-seq peaks (Figure 1E).

Trends underlying observed differential CTCF HiChIP interactions could also be observed in Hi-C data from THP-1 cells treated with $1,25(OH)_2D_3$. Viewpoint analyses of differential CTCF HiChIP anchors revealed that even at a shallow sequencing depth, a number of differential CTCF HiChIP interactions were also observable when not only focusing on interactions mediated by CTCF (Supplementary figures S4A–C).

Taken together, 3.1% of all CTCF-mediated chromatin loops in monocytic THP-1 cells are sensitive to VDR activation and the overrepresented upregulated loops are enriched for promoter-enhancer interactions.

$1,25(OH)_2D_3$ treatment changes chromatin conformation close to TAD boundaries

As CTCF binding is important for the formation of TADs, we sought to examine whether VDR activation leads to changes in chromatin domain organization, such as the frequency of individual TADs in a cell. We intersected differential CTCF loops with published TADs called from DLO Hi-C data in THP-1 cells (101). We found that the anchors of differential CTCF loops were significantly enriched for TAD borders when compared to shuffled loops, but not when compared to stable loops (Supplementary Figure S5A, $P < 0.001$, Fisher's Exact Test). The locus of the vitamin D target gene zinc finger protein 618 (*ZNF618*) is a representative example, where a differential CTCF interaction coincides with a TAD (Supplementary Figure S5B).

To further develop this finding, we used differential TAD border detection to identify whether any differential CTCF HiChIP loops matched modulated TADs observed in our own Hi-C data from vehicle- and $1,25(OH)_2D_3$-treated THP-1 cells. Of the 8,215 TAD borders identified by TADCompare, 1,700 were classified as differential with different consequences on the TADs they defined (745 complex, 493 split, 429 merged, 33 changed in strength) (Supplementary Figure S6A). Representative examples of differential TADs, which reflected putative differential CTCF HiChIP loops, were those in the loci of the vitamin D target genes androgen induced 1 (*AIG1*), adenosine deaminase tRNA specific 2 (*ADAT2*) and cytochrome P450 family 24 subfamily A member 1 (*CYP24A1*), where differential loop anchors clearly intersected with TAD boundaries enriched after $1,25(OH)_2D_3$ treatment (Supplementary Figures S6B and C).

This indicates that VDR-mediated changes of chromatin interactions may affect CTCF-marked TAD boundaries.

VDR binding sites are enriched at $1,25(OH)_2D_3$-responsive CTCF loop regions

To elucidate the interplay between VDR and CTCF-defined chromatin structure, we integrated previously published VDR ChIP-seq data (99) with differential loops. Of special interest was the identification of differential loops where VDR binding in proximity to the loop anchor regions could affect differential loop formation or VDR promoter-enhancer interactions. VDR ChIP-seq peaks were enriched in proximity of differential CTCF loop anchors when compared to shuffled and stable loop sets (Figure 2A):

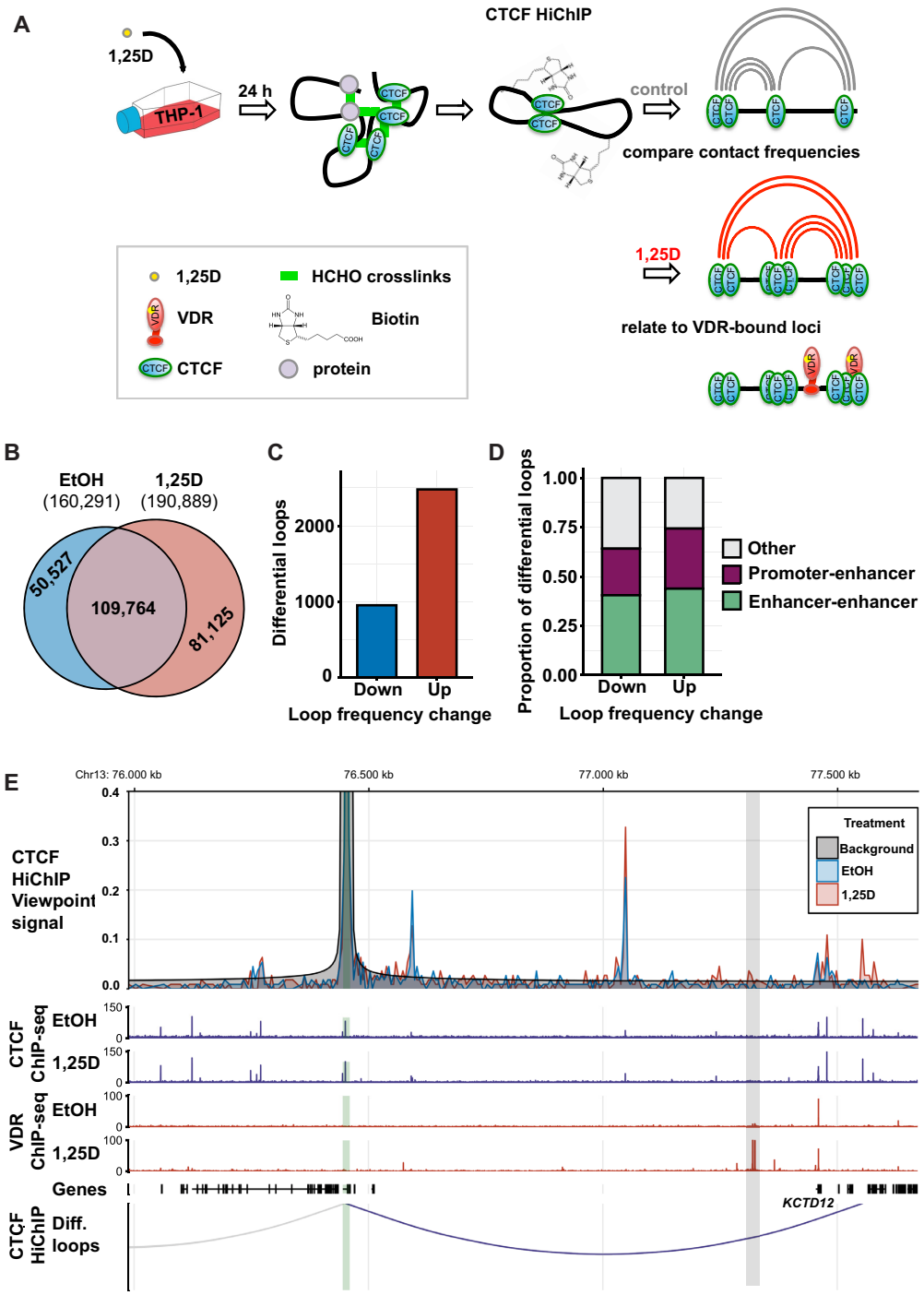

Figure 1. Treatment of THP-1 cells with $1,25(OH)_2D_3$ provoked changes in CTCF-directed chromatin conformation, identified by differential chromatin topology analysis of HiChIP data. (**A**) Experimental setup of this study. THP-1 cells were treated for 24 h with 100 nM $1,25(OH)_2D_3$ or control (EtOH). Triplicate CTCF HiChIP experiments were performed and the interactions were called using *hichipper*. The resulting loop data was integrated with previous VDR ChIP-seq data (99). (**B**) Intersect between consistent (i.e. present in all three replicates) CTCF loops in control and $1,25(OH)_2D_3$-treated cells. (**C**) Numbers of upregulated and downregulated differential (Padj < 0.05, *diffloop*) loops in $1,25(OH)_2D_3$ treatment versus control (vehicle) HiChIP samples. (**D**) Annotation of upregulated and downregulated differential CTCF loops as enhancer-enhancer, promoter-enhancer, or other loops (see Supplementary Figures S3A–D for all types). Enhancers were taken from *EpiRegioDB*, and promoters were considered as a 5 kb (2.5 kb upstream/downstream) window around the TSSs of all hg19 genes. (**E**) Virtual 4C viewpoint analysis of a differential loop anchor region in both control and $1,25(OH)_2D_3$-treated cells (n = 3, summed interaction frequencies), shown alongside CTCF ChIP-seq (violet tracks, (73,79)) and VDR ChIP-seq (red tracks, (99)) data. There are two strong $1,25(OH)_2D_3$-induced VDR peaks (shaded in grey) in the locus, while the strong VDR site at the TSS of the vitamin D target gene *KCTD12* (24 h $1,25(OH)_2D_3$: $\log_2$ FC $=$ 3.44; $P_{adj} < 0.001$) is persistently occupied with and without $1,25(OH)_2D_3$ stimulation.

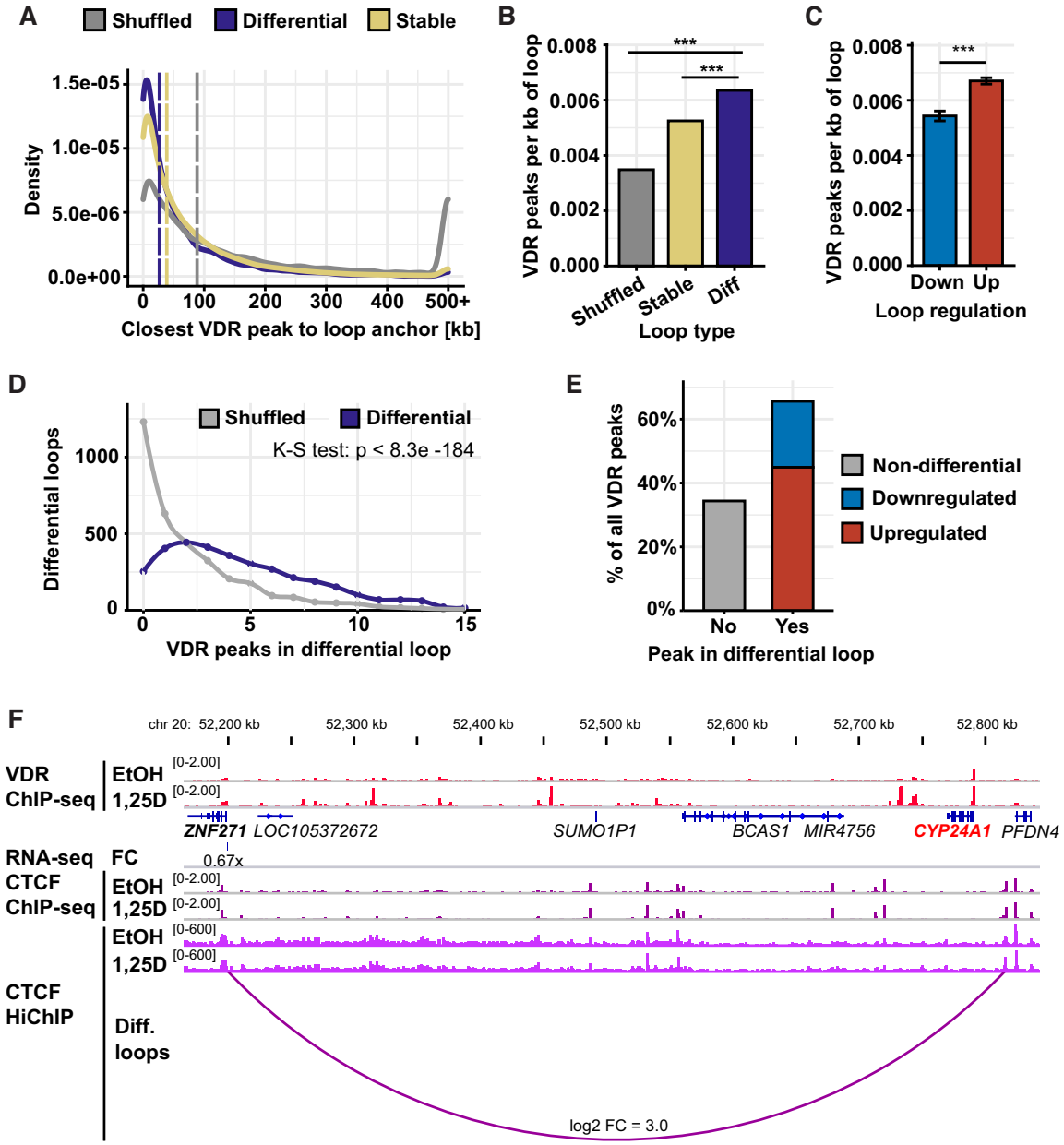

Figure 2. VDR binding loci were enriched inside differential CTCF loops and preferentially located close to differential CTCF loop anchors. (**A**) Densities of the minimum linear distances between differential, stable, and shuffled differential loop anchors and VDR ChIP-seq peaks (99). The dashed lines represent the median distances per loop set. (**B**) Occurrence rate of previously identified VDR ChIP-seq peaks (99) present in THP-1 cells after 24 h of 100 nM $1,25(OH)_2D_3$ treatment per kb of differential, stable and shuffled loops. The difference between the regions was computed using Fisher's exact test for shuffled loops, and the proportion of stable loop sets, which exceeded the differential value for stable loops. The standard deviations are too small to be visible. (**C**) Number of VDR ChIP-seq peaks per kb of upregulated and downregulated loops. (**D**) Numbers of shuffled and differential CTCF loop regions containing different numbers of VDR ChIP-seq peaks (99). Difference between the two distributions was determined using a two-sided Kolmogorov–Smirnov (K–S) test. There were 2,231 differential CTCF loops intersecting with more than two VDR peaks versus 1,131 shuffled loop regions. (**E**) Percentage of all 9,763 VDR ChIP-seq peaks (99) intersecting with either upregulated differential CTCF loops (44.9%), downregulated differential CTCF loops (20.7%), or not intersecting with any differential CTCF loop (34.4%). (**F**) An upregulated differential CTCF loop (violet arc) in the locus of the strong vitamin D target gene *CYP24A1* contains several VDR sites (red peak tracks) (99), one of which is located within 25 kb distance of one of the loop anchors. Gene structures are shown in blue. The violet peak track displays CTCF ChIP-seq data (73,79) and CTCF HiChIP peaks. The expression change (FC, linear fold change) 24 h after stimulation with $1,25(OH)_2D_3$ as determined by RNA-seq (73,99) is given for significant DEGs. The scale for the VDR peak tracks has been chosen such as so allow weaker peaks to be visible, which is why the summit of strong peaks is cut.

differential CTCF loops, stable CTCF loops, and shuffled loops had median loop anchor-VDR distances of 26.7, 38.7 and 88.4 kb, respectively.

To also characterize those differential loops, which were not putative promoter-enhancer interactions, we then analyzed whether VDR peaks were located inside $1,25(OH)_2D_3$-modulated loops. The number of VDR peaks per kb of loop was significantly greater in differential loops (0.0064) when compared to stable (0.0053) and shuffled (0.0035) loop sets ($P < 0.05$, Fisher's exact test for shuffled, proportion exceeded for stable) (Figure 2B). The enrichment of VDR peaks was higher in upregulated than in downregulated loops (Figure 2C). There were also significantly more instances of multiple VDR peaks intersecting with differential loop regions, compared to shuffled loop regions (Figure 2D). Of the 9,763 VDR peaks used in the analysis, 4,386 (44.9%) lay within upregulated differential CTCF loops and 2,020 (20.7%) within downregulated loops (Figure 2E).

The locus of the vitamin D target gene *CYP24A1* illustrates a differential loop, containing a DEG and several strong VDR binding sites. *CYP24A1* is located closely (~25 kb distance) to one of the loop anchors (Figure 2F).

In summary, VDR binding sites are preferentially located in CTCF loops that are modulated by $1,25(OH)_2D_3$ treatment.

VDR-dependent gene expression is linked to dynamic CTCF-loops

To elucidate whether the observed VDR-dependent changes in CTCF-mediated loops correlate with changes in gene expression, we incorporated previously published RNA-seq data (73,99). The number of DEGs observed per kb of loop was significantly ($P < 0.05$, Fisher's exact test for shuffled, proportion exceeded for stable) greater in differential loops (0.0024) when compared to stable (0.0018) and shuffled (0.0013) loop sets (Figure 3A). The majority of the 3,372 differentially expressed genes after $1,25(OH)_2D_3$ stimulation (2,272, 67.4%) resided inside differential CTCF loops (Figure 3B). Significantly more differential CTCF loops contained multiple DEG loci when compared to shuffled loops (Figure 3C). Along the same lines, the co-occurrence of DEGs and VDR peaks was enriched in differential CTCF loops (Figure 3D). DEGs and VDR loci co-occurred in 73.3% and 58.8% of upregulated and downregulated differential CTCF loops, respectively (Figure 3E). Interestingly, predicted primary VDR target genes (100) were enriched inside differential CTCF loops. Of DEGs residing within differential CTCF loops, 64.5% were predicted primary VDR targets. This was significantly different ($P < 4.915e{-}15$, Fisher's exact test) compared to only 50.4% direct VDR targets of the DEGs located outside of differential loop regions (Figure 3F).

Similar to VDR binding sites, DEGs were located close to differential loop anchors, indicating that the interaction of VDR at CTCF-loop anchors is important for the regulation of associated target genes (Figure 3G).

A differential loop containing eight vitamin D target genes and several VDR-bound sites is an example for the above observations (Figure 3H). The highly $1,25(OH)_2D_3$-responsive gene *CD14* and several VDR sites were in close proximity to the loop anchors.

These data show that primary vitamin D target genes are enriched in differential loops and tend to be close to their anchors. A high proportion of the $1,25(OH)_2D_3$-sensitive CTCF loops contain both VDR site(s) and DEG(s).

$1,25(OH)_2D_3$-sensitive CTCF loops are enriched in VDR or downstream transcription factor binding at anchor regions

Our previous analyses suggested a prominent role of VDR binding in the vicinity of loop anchor regions in differential CTCF-looping. However, VDR binding may occur at other regulatory genes that work downstream of VDR to regulate gene expression (100). To gauge whether differential CTCF loops can also be a consequence of association of the previously identified 47 downstream transcription factors (100), we used VDR and ETS1 ChIP-seq and FAIRE-seq data (73) in combination with transcription factor binding prediction (90).

More than half (55.3%) of the differential CTCF loops had a VDR ChIP-seq peak or a predicted VDR/VDR:RXRA binding motif in a FAIRE-seq peak within 25 kb of at least one of their loop anchors. This enrichment was even stronger when considering only upregulated loops (59.0%) (Figure 4A). VDR was shown to bind at 48.3% (1,658) of all 3,433 differential loops. At anchors of an additional 240 differential loops VDR binding was only predicted by motif occurrence, while at the remaining 1,534 loops there was no obvious VDR binding event at their anchor regions. VDR-downstream transcription factors, encoded by primary vitamin D target genes, were predicted to bind at 76.7% (1,176) of these (100). Indeed, of all differential CTCF loops, only 10.5% (359) did not have a VDR peak, predicted VDR/VDR:RXRA, or downstream VDR target transcription factor motif at their loop anchor regions (Figure 4B). Among the downstream transcription factors with the highest enrichment in predicted affinity at differential loop anchors were E2F transcription factor 4 (E2F4) and zinc finger and BTB domain containing 7A (ZBTB7A) (Figure 4C). As expected, predicted CTCF binding correlation with loop frequency change was highest, while VDR:RXR ranked seventh in the list of transcription factors. Some downstream transcription factors tended to appear less in differential loop anchors (Supplementary Figure S7). Using previously published ChIP-seq data for the transcription factor ETS1 (100), we could validate the predicted enrichment of ETS1 at anchors of differential loops (Figure 4D).

The possible scenarios of $1,25(OH)_2D_3$-modulated CTCF interactions that can be deduced from our analyses include VDR enhancer-promoter interactions. VDR may associate to one of the CTCF loop anchors, while the TSS of its target gene is located at the other loop anchor (Figure 4E). In contrast, VDR may also interact with the TSS of the primary DEG independently from CTCF, while the frequency of the CTCF-formed insulated neighborhood or TAD is influenced by the colocation of VDR (Figure 4F) or a downstream transcription factor (Figure 4G) to one of

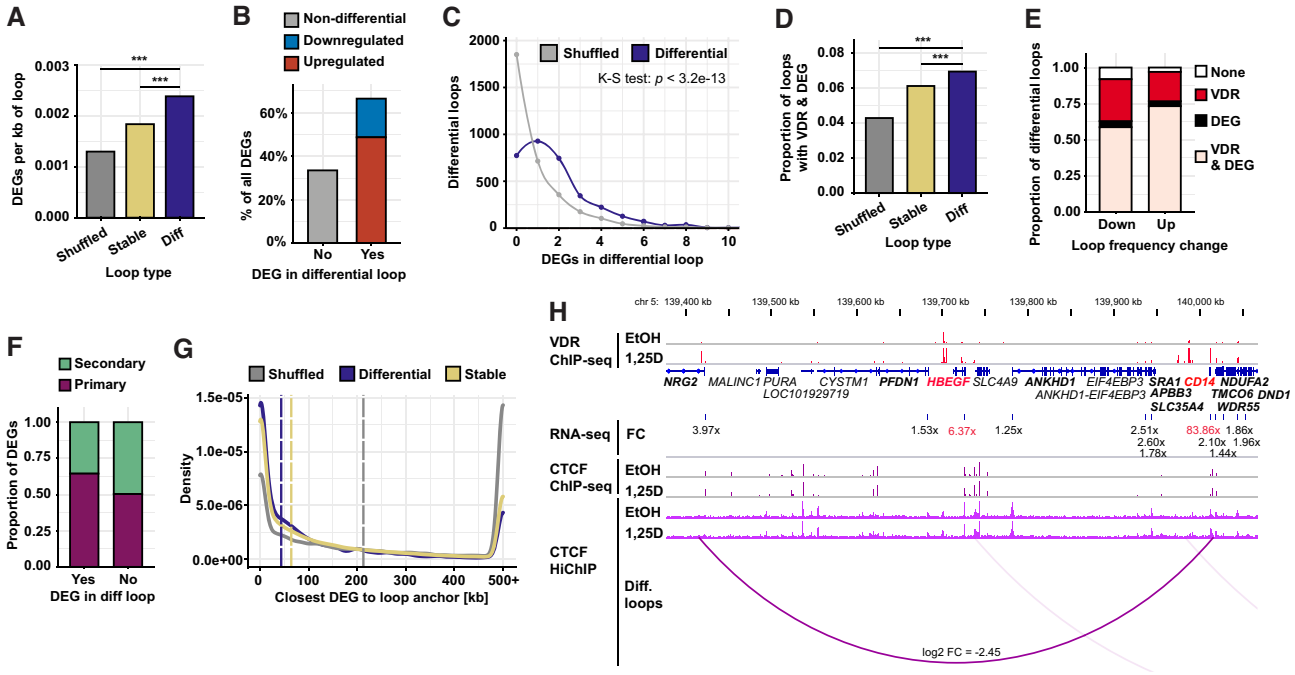

Figure 3. $1,25(OH)_2D_3$-responsive genes were enriched inside differential CTCF loops and close to differential CTCF loop anchor regions. (**A**) Occurrence rate of $1,25(OH)_2D_3$-responsive gene loci in differential, stable, and shuffled differential loops. The difference between the loop types was computed using a Fisher's exact test for shuffled loops, and the proportion of stable loop sets which exceeded the differential value for stable loops. (**B**) Percentages of genes previously identified as being differentially expressed after 24 h $1,25(OH)_2D_3$ treatment in THP-1 cells where the gene loci intersected with upregulated differential CTCF HiChIP loops, downregulated differential CTCF HiChIP loops, or which did not intersect with any differential loop. (**C**) Numbers of differential CTCF HiChIP loops and shuffled differential loops intersecting with different numbers of $1,25(OH)_2D_3$-responsive genes (73,99). Difference between the distributions was evaluated using a two-sided Kolmogorov–Smirnov (K–S) test. Overall, 1,605 differential CTCF loops contained more than one DEG, in contrast to 741 shuffled loops. (**D**) Proportions of differential, stable, and shuffled loops, which intersected with both a $1,25(OH)_2D_3$-responsive gene (73,99) and a VDR ChIP-seq peak (99) present in THP-1 cells after $1,25(OH)_2D_3$ treatment. The difference between the loop sets was computed using Fisher's exact test for shuffled loops, and the proportion of stable loop sets, which exceeded the differential value for stable loops. (**E**) Proportions of upregulated and downregulated differential CTCF HiChIP loops which intersected with either $1,25(OH)_2D_3$-responsive genes (73,99), VDR ChIP-seq peaks (99), both features, or neither feature. (**F**) Relative proportions of $1,25(OH)_2D_3$-responsive genes (73,99) that intersected with differential CTCF HiChIP loop regions, which were previously classified as either being directly regulated by VDR (primary vitamin D target gene) or as being regulated by transcription factors downstream of VDR (secondary target) (100). The enrichment of primary vitamin D target genes in differential loops was significant ($P < 4.915e{-}15$, Fisher's exact test). (**G**) Densities of minimum linear distances between differential, stable, and shuffled CTCF HiChIP loop anchors and $1,25(OH)_2D_3$-responsive gene loci (73,99): median distances were 150 kb (upregulated loops), 211 kb (downregulated loops) and 524 kb (shuffled loops). (**H**) Representative example of a $1,25(OH)_2D_3$-sensitive CTCF loop (violet arc) containing eight vitamin D target genes, among them *CD14* and *HBEGF*, together with several VDR ChIP-seq peaks (99). Four DEGs and four VDR sites (red peak tracks) are in proximity (within 25 kb) of either loop anchor. Gene structures are shown in blue. The violet peak track displays CTCF ChIP-seq data (73,79) and CTCF HiChIP peaks (lighter violet). The expression change (FC, linear fold change) 24 h after stimulation with $1,25(OH)_2D_3$ as determined by RNA-seq (73,99) is given for significant DEGs. The scale for the VDR peak tracks was chosen to enable visualization of weaker peaks, thus the summit of strong peaks is cut.

the CTCF loop anchors. Correspondingly, the binding of a VDR-regulated transcription factor at one CTCF loop anchor may facilitate its contact with the TSS of its target gene located at the other CTCF loop anchor (Figure 4H). A downstream transcription factor residing in a differential CTCF loop with VDR at its anchors may contact the TSS of a secondary vitamin D target gene independently from CTCF (Figure 4I). Finally, VDR may also be present in the loop without directly regulating the secondary vitamin D target gene (Figure 4J). Differential CTCF HiChIP loops were assigned to one or more of the aforementioned categories, with the majority falling under putative VDR transcriptional neighborhoods bounded by CTCF with or without VDR or a downstream transcription factor binding at one of the loop anchors (Figures 4E–J and Supplementary Table S5).

In summary, the majority of all differential CTCF loops can be linked to the presence of VDR or directly VDR-regulated transcription factors in the respective loops.

VDR promoter-enhancer loops are facilitated by CTCF-CTCF interactions

In order to determine functional consequences of VDR/CTCF promoter-enhancer loops, we performed CRISPRi experiments in THP-1 cells. The locus of the vitamin D target gene jagged canonical Notch ligand 1 (*JAG1*) contains three CTCF loops which were not called differential, but were consistently present only after the $1,25(OH)_2D_3$ treatment (Figure 5A). One of them represented a putative VDR enhancer-promoter interaction as VDR co-located to one loop anchor while the *JAG1* TSS was located at the other anchor. Inside the loop there were some additional VDR sites, one of them being much stronger than the one at the loop anchor. Thus, this

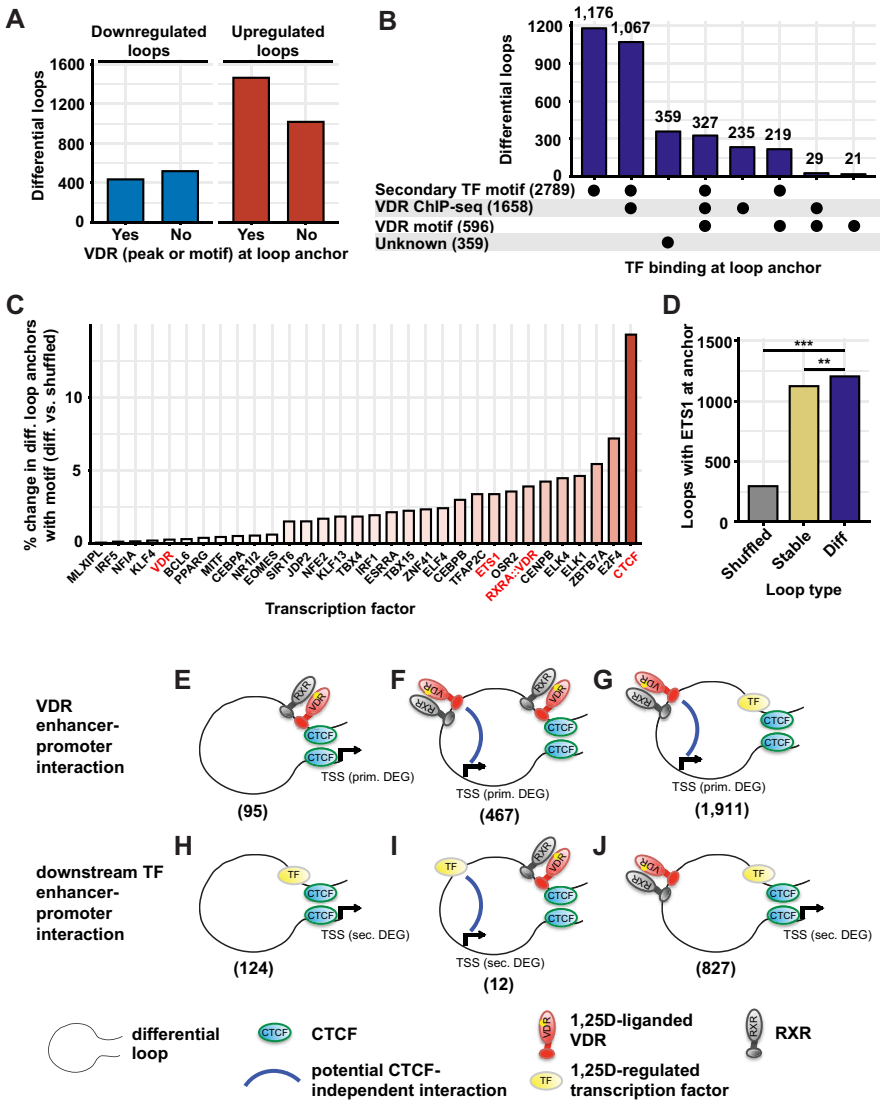

Figure 4. Most differential CTCF HiChIP loop anchor regions intersected with either VDR binding sites, or binding motifs of transcription factors downstream of VDR. (**A**) The number of the upregulated (in total 2,480) and downregulated (in total 980) differential CTCF HiChIP loops where either a VDR ChIP-seq peak (99) or a VDR/VDR:RXRA binding motif was or was not identified in at least one loop anchor region. (**B**) An upset plot characterizes the sets of differential CTCF HiChIP loops where a VDR ChIP-seq peak (1,658), VDR/VDR:RXRA binding motif (596), or downstream transcription factor binding motif (2,789) was present in either of the loop anchor regions. In total, VDR peaks or its binding motif were identified at an anchor of 1,898 differential loops. At 1,534 1,25$(OH)_2D_3$-sensitive loops no VDR binding was shown (ChIP-seq (99)) or predicted (motif), but at 1,176 of these association of a 1,25$(OH)_2D_3$-regulated transcription factor was predicted. Loops where none of the features were present were designated as unknown (359). (**C**) Percentage change in the numbers of differential CTCF loop anchors predicted to be bound by CTCF, VDR, VDR:RXRA or transcription factors previously identified to be primary targets of VDR, relative to shuffled loops. (**D**) The number of differential, stable, and random (shuffled) CTCF HiChIP loops where an ETS1 ChIP-seq peak (100) was detected in at least one loop anchor region. Difference was evaluated using a Fisher's exact test. (**E–J**) Models depicting different potential scenarios involving VDR/RXR or downstream transcription factors bound at differential loops in the regulation of primary and secondary vitamin D target genes. The frequency of each model among the differential CTCF loops is indicated below the respective model.

locus represents a more complex variation of the model in Figure 4E (Supplementary Figure S8A). It was primarily chosen to validate our CRISPRi system by targeting both the TSS and a strong enhancer of a VDR target gene. Thus, we first designed gRNAs targeting either the TSS of the *JAG1* gene or the strong VDR site in ≈ 170 kb distance of the TSS (Figure 5C and D). Targeting the dCas9-KRAB fusion protein to the *JAG1* TSS significantly reduced the basal and stimulated *JAG1* mRNA levels by 39.8% and 44.7%, respectively (Figure 5F). CRISPRi for the strong VDR enhancer significantly reduced mainly the 1,25$(OH)_2D_3$-stimulated *JAG1* expression by 28.9% (L98) up to 63.3% (L99) (Figure 5F, Supplementary Figure S8B). The induction of *JAG1* mRNA expression by 1,25$(OH)_2D_3$ was also decreased when targeting the strong VDR site (Supplementary Figure S8C). The distal loop anchor region contained both a VDR and a CTCF site (Figure 5B). These results confirmed that our CRISPRi system works fine. In contrast to the inhibitions observed at the *JAG1* TSS and strong VDR enhancer, CRISPRi targeting both the VDR

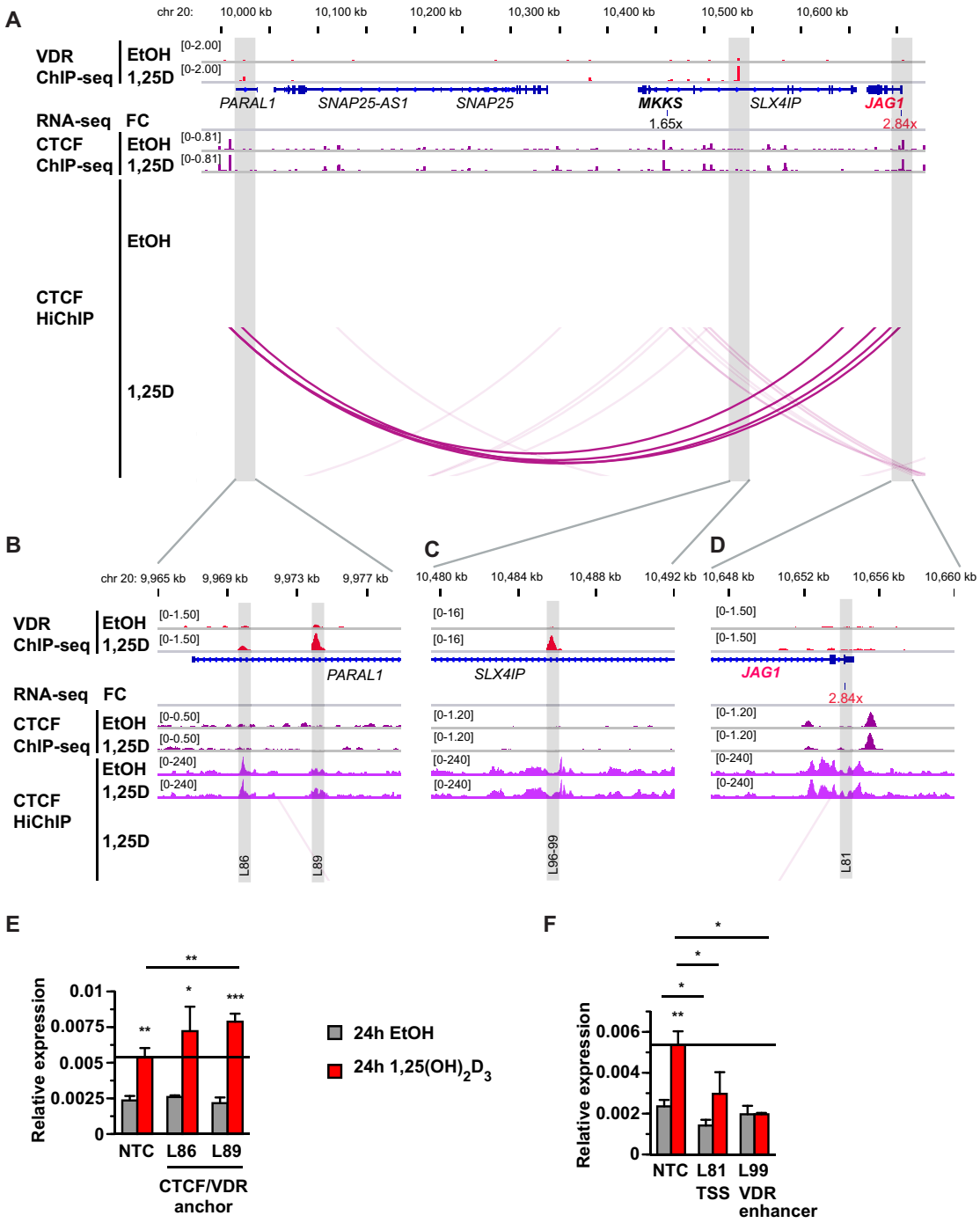

Figure 5. CRISPRi identified a strong VDR enhancer in the *JAG1* locus regulating *JAG1*, while the functionality of a distal VDR/CTCF site that interacted with the CTCF anchor at the *JAG1* TSS remained uncertain. (**A**) A CTCF HiChIP loop (violet arcs) in the *JAG1* locus, which was present consistently only after stimulation with $1,25(OH)_2D_3$, represents a potential VDR enhancer-promoter interaction as VDR co-located to one of the loop anchors, while the TSS of the vitamin D target *JAG1* was located at the other anchor. Both loop anchors as well as a strong VDR ChIP-seq peak (red peak tracks) (99) inside of the loop are marked by a grey shade. Gene structures are shown in blue. The violet peak tracks display CTCF ChIP-seq data (73,79), as well as the CTCF HiChIP peaks (lighter violet). The expression change (FC, linear fold change) 24 h after stimulation with $1,25(OH)_2D_3$ as determined by RNA-seq (73,99) is given for significant DEGs. The scale for the VDR peak tracks has been chosen such as so allow weaker peaks to be visible, which is why the summit of strong peaks is cut. (**B-D**) Zoomed-in representations of the regions to which the CRISPRi experiments were targeted. (**E**) Lentiviral CRISPRi using two different gRNAs targeting the distal CTCF/VDR site (L86 and L89) or a non-targeting control (NTC) followed by stimulation was performed with THP-1 cells. After the transduction, the cells were treated for 24 h with $1,25(OH)_2D_3$ or EtOH, followed by RT-qPCR experiments for *JAG1*. (**F**) Lentiviral CRISPRi using one gRNA targeting the *JAG1* TSS (L81), a gRNA targeting the strong VDR site (L99), or NTC. Transduction, stimulation and RT-qPCR for *JAG1* were performed as described for (E). Columns in (E) and (**F**) represent the means of three independent experiments and the bars indicate standard deviations. Two-tailed Student's *t*-tests were performed to determine the significance of the mRNA induction by $1,25(OH)_2D_3$ in reference to solvent-treated cells and of expression changes compared to the NTC control cells (* $P < 0.05$; ** $P < 0.01$; *** $P < 0.001$).

(L86) and the CTCF (L89) site in the anchor region led to an increased 1,25$(OH)_2D_3$-stimulated *JAG1* expression by 34.5% and 46.9%, respectively (Figure 5E). The neighbor gene *SLX4IP* was not affected by the CRISPRi, proving the specificity of the used gRNAs (Supplementary Figure S8D).

VDR also associated to a CTCF loop anchor region interacting with the TSS of the *PTGES2* gene, which is located at the other anchor (Figure 6A, Supplementary Figure S9A). The frequency of this differential loop was increased ($\log_2$ FC = 2.5) after 1,25$(OH)_2D_3$ treatment. As there were several VDR sites and seven DEGs in the differential loop, also this region represents a complex variation of the model in Figure 4E. Similarly as in the *JAG1* locus, the distal loop anchor region contained both a VDR and a CTCF site (Figure 6B). CRISPRi with three of the six tested gRNAs led to a modest but significant reduction of 1,25$(OH)_2D_3$-stimulated *PTGES2* expression (−14.3%, −17.0% and −16.1% for L90, L93 and L95, respectively) (Figure 6C, Supplementary Figure S9B and C). The gRNAs were shown to be specific for *PTGES2* by the neighbor gene *SLC25A25* being unaffected by the CRISPRi (Supplementary Figure S9D).

Taken together, a distal VDR/CTCF enhancer regulated the *PTGES2* gene and its interaction with the TSS was facilitated by a differential CTCF loop. Thus, CTCF loops support precise gene regulation by the VDR. In the *JAG1* locus, CRISPRi identified a strong VDR site in a 1,25$(OH)_2D_3$-gained loop as its functional enhancer. A more distal VDR site looped together with CTCF to the other CTCF anchor at the *JAG1* TSS, but the functionality of it as VDR/CTCF enhancer was uncertain.

The maintenance of some vitamin D-sensitive CTCF-CTCF loops containing VDR site(s) and DEG(s) is required for a complete transcriptional response to 1,25$(OH)_2D_3$

Aiming to elucidate the impact of 1,25$(OH)_2D_3$-modulated long-range CTCF interactions, we used the CRISPR/Cas9 gene editing technology to delete the anchors of some representative differential loops.

We have identified three 1,25$(OH)_2D_3$-modulated CTCF loops in the locus of the two neighboring vitamin D target genes *ADAMDEC1* and ADAM metallopeptidase domain 28 (*ADAM28*) (Figure 7A). Of two of them, we deleted one anchor, each. In roughly 2 kb distance to one of the two deleted loop anchors VDR was shown to bind (Supplementary Figure S10A), while there were no VDR ChIP-seq peaks close to the other anchor (Supplementary Figure S10B).

We performed RT-qPCR experiments with four single cell clones from two different gRNA combinations (L59 and L60) carrying the homozygous deletion of the left loop anchor. In the best clone (L60-F6) the 1,25$(OH)_2D_3$-induced *ADAMDEC1* and *ADAM28* mRNA expressions were significantly reduced compared to the NTC control by 62.4% and 63.7%, respectively (Figure 7B, Supplementary Figures S11A–D). In contrast, there were no significant expression changes of three non-vitamin D-responsive genes inside and outside the differential loop.

Effects of the deletion of the right anchor of the second differential loop in the *ADAMDEC1* locus were studied for two deletion cell lines (L66 and L67). The 1,25$(OH)_2D_3$-stimulated expression levels of both *ADAM28* and *ADAMDEC1* were reduced in both lines compared to the control cell line (Figure 7C, Supplementary Figure S12). For the best deletion line (L67), *ADAMDEC1* and *ADAM28* expressions were significantly reduced by 49.7% and 41.3%, respectively (Supplementary Figure S12C). The non-DEGs dedicator of cytokinesis 5 (*DOCK5*) and gonadotropin releasing hormone 1 (*GNRH1*) were both located downstream of the deleted right loop anchor. Following the anchor deletion, *GNRH1* gained 1,25$(OH)_2D_3$ responsiveness, as shown by the significant increase (62%) of 1,25$(OH)_2D_3$-stimulated *GNRH1* expression compared to the control cell line (Figure 7C) and by the increased fold changes for both deletion lines (Supplementary Figure S12A).

The vitamin D target gene potassium voltage-gated channel modifier subfamily F member 1 (*KCNF1*) is located in a differential loop together with several VDR-bound loci, but no VDR bound within ±25 kb of either loop anchor (Supplementary Figure S13A–C). Instead, the downstream transcription factor ETS1 was shown to associate to the right boundary site. The induction by the VDR ligand was impaired (decreased fold change) after deletion of the left loop anchor (Supplementary Figure S14B). Two genes outside the differential loop either lost their response to 1,25$(OH)_2D_3$ (ribonucleotide reductase regulatory subunit M2 (*RRM2*)) or even turned from a downregulated gene to an upregulated gene (Rho associated coiled-coil containing protein kinase 2 (*ROCK2*)) by the left anchor deletion.

Deletion of another differential CTCF loop containing the vitamin D target gene TNF receptor associated factor 5 (*TRAF5*) and two VDR ChIP-seq peaks led to only weak and mostly non-significant changes of 1,25$(OH)_2D_3$ regulation inside and outside the loop (data not shown).

In summary, the deletion of four different anchors of four differential loops led to an impaired vitamin D induction of vitamin D target genes inside the respective loop. Also, the CTCF loop anchor deletion caused a gain, loss or increase of vitamin D responsiveness of some genes outside of the 1,25$(OH)_2D_3$-sensitive loops.

DISCUSSION

Here, we report the first genome-wide dataset of CTCF long-range interactions in 1,25$(OH)_2D_3$-treated cells and examined the interplay between activated VDR and transcription factor-specific changes in chromatin conformation. To our knowledge no comparable study has been done for most other nuclear receptors. Hi-C and 5C data have been generated from estrogen-treated cells (103) and another study generated Hi-C datasets from estrogen-resistant and -sensitive breast cancer cells, but did not include estrogen stimulations (78). Recently, published H3K4me3-HiChIP data were used in combination with transcription factor ChIP-seq data to characterize regulatory domains controlling expression of the mouse and human *VDR* gene in the intestine. This study did not include any 1,25$(OH)_2D_3$

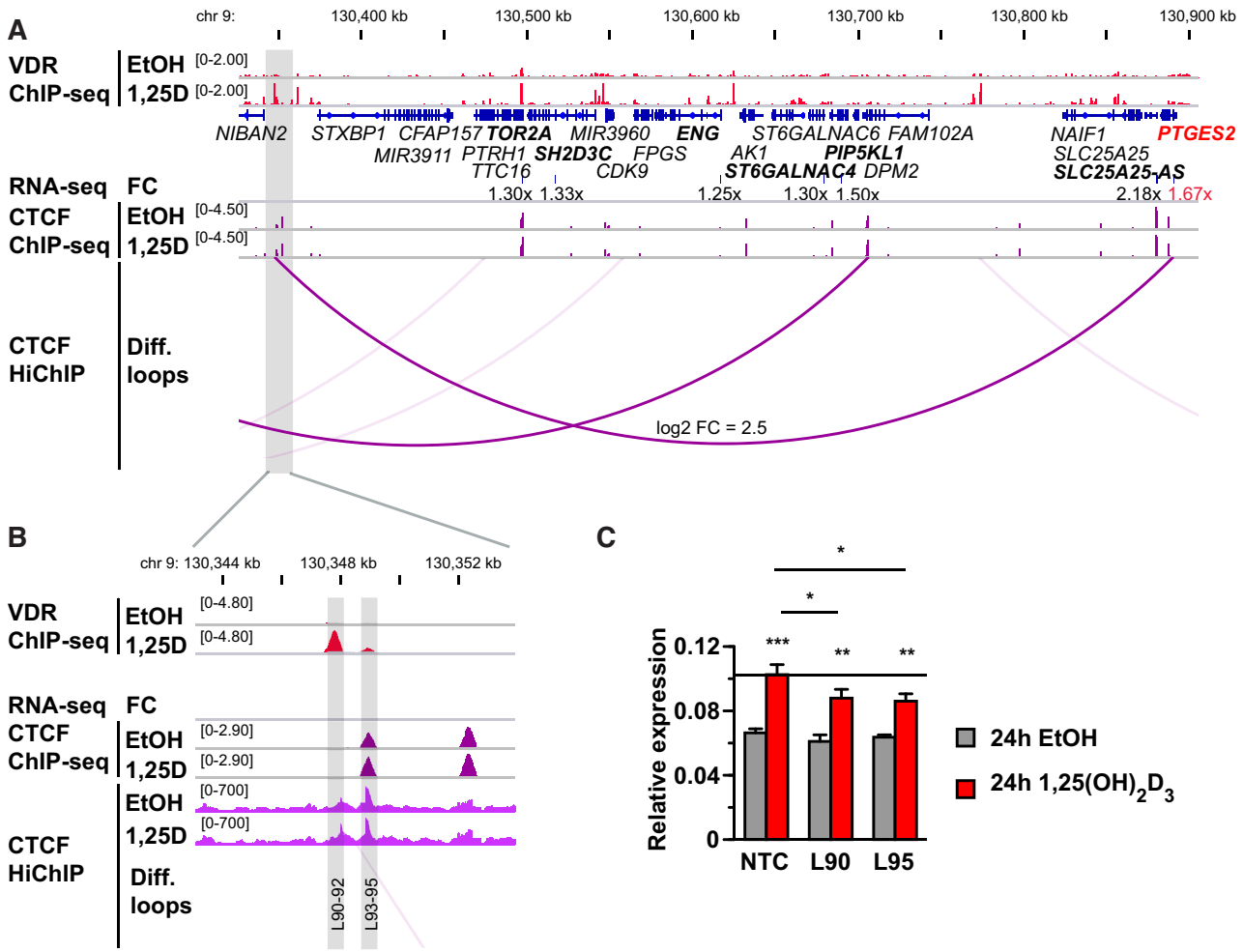

Figure 6. The anchor of a $1,25(OH)_2D_3$-upregulated CTCF loop was shown to be a functional VDR enhancer regulating *PTGES2*. (**A**) A differential CTCF HiChIP loop (violet arc) in the *PTGES2* locus represents a potential VDR enhancer-promoter interaction as VDR co-located to one of the loop anchors while the TSS of the vitamin D target *PTGES2* was located at the other anchor. The VDR ChIP-seq and CTCF ChIP-seq data are displayed in the red and violet peak tracks, respectively (73,79,99). CTCF HiChIP peaks tracks are displayed in the lighter violet tracks. The CTCF/VDR loop anchor is marked by a grey shade. Gene structures are shown in blue. The expression change (FC, linear fold change) 24 h after stimulation with $1,25(OH)_2D_3$ as determined by RNA-seq (73,99) is given for significant DEGs. The scale for the VDR peak tracks has been chosen such as so allow weaker peaks to be visible, which is why the summit of strong peaks is cut. (**B**) Zoomed-in representation of the region to which the CRISPRi experiments was targeted. (**C**) Lentiviral CRISPRi for the best two of six tested gRNAs targeting the distal CTCF/VDR site (L90, L95) or a non-targeting control (NTC), was performed with THP-1 cells. Subsequently, the cells were treated for 24 h with $1,25(OH)_2D_3$ or solvent and RT-qPCR assays were carried out. Columns represent the means of three independent experiments and the bars indicate standard deviations. Two-tailed Student's t-tests were performed to determine the significance of the mRNA induction by $1,25(OH)_2D_3$ in reference to solvent-treated cells and of expression changes compared to the NTC control cells (* $P < 0.05$; ** $P < 0.01$; *** $P < 0.001$).

treatments either (104). Activation of a nuclear receptor as a ligand-activated transcription factor provides an excellent non-steady state model system to investigate dynamic changes in genome topology. Given that CTCF is an important protein for the establishment of 3D chromatin structure, and that CTCF binding is modulated by $1,25(OH)_2D_3$ (73,79), we performed CTCF HiChIP assays to identify CTCF-specific changes in chromatin topology. Unlike many other publications, we focused on the statistically proven differential interactions arising from multiple biological replicates. Without this approach, there would have appeared to be 1,680,769 loops which were either lost or established de novo after $1,25(OH)_2D_3$ treatment. However, due to very low contact frequencies, 99.9% (1,678,994) of the lost and *de novo* loops were not called as differential by *diffloop*, reflecting the possibility that these are artefacts and not true *de novo* interactions. Contrastingly, 3% of the consistent CTCF loops (present in all three replicates of both treated and untreated cells) were significantly changed by the VDR ligand, reflecting how more robust count data supports calling of differential features. Our results revealed that the majority of all vitamin D target genes are located in $1,25(OH)_2D_3$-sensitive loops, supporting the common notion that enhancers and target promoters are co-located in a TAD or sub-TAD to facilitate robust and precise gene expression regulation. The observed enrichment of multiple

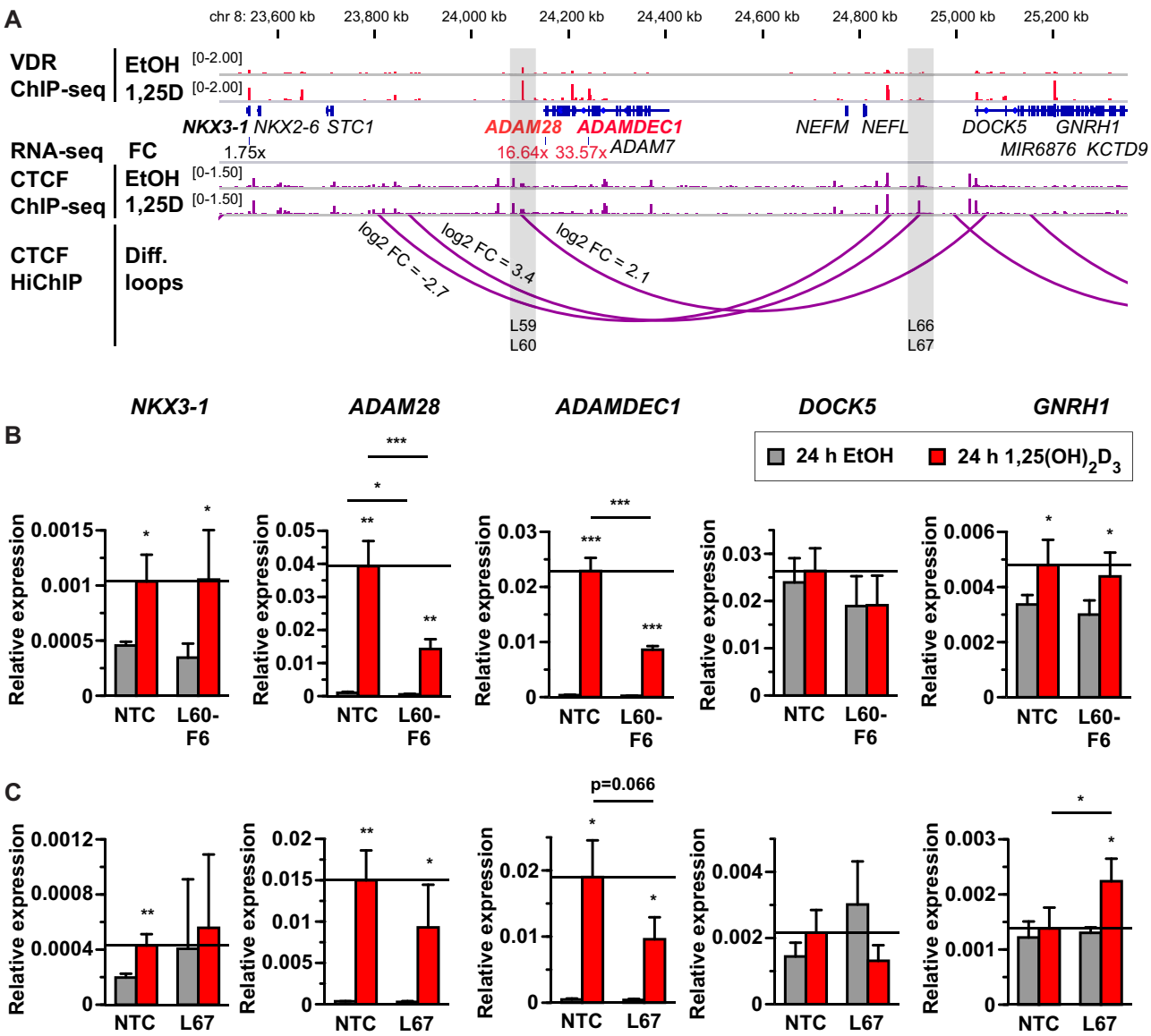

Figure 7. Disruption of $1,25(OH)_2D_3$-sensitive CTCF loops in the *ADAM28/ADAMDEC1* locus impaired normal up-regulation of the vitamin D target genes in the loop and increased the response of a gene outside of the loop. (**A**) CTCF HiChIP assays identified three $1,25(OH)_2D_3$-modulated CTCF loops (violet arcs) in the *ADAM28/ADAMDEC1* locus. VDR located close to two of the six loop anchors (red peak tracks) (99) and two anchors were selected for deletion (marked by grey shading). The CTCF ChIP-seq is displayed in the violet peak tracks (73,79), as well as the CTCF HiChIP peaks (lighter violet). Gene structures are shown in blue. The expression change (FC, linear fold change) 24 h after stimulation with $1,25(OH)_2D_3$ as determined by RNA-seq (73,99) is given for significant DEGs. The scale for the VDR peak tracks has been chosen such as so allow weaker peaks to be visible, which is why the summit of strong peaks is cut. (**B**) CRISPR/Cas9 gene editing was utilized to delete the left shaded CTCF loop anchor region. A combination of two different gRNAs cloned into vectors conveying puromycin or hygromycin resistance to allow for double selection after the lentiviral transduction of THP-1 cells. Three single cell clones obtained from two different gRNA combinations (L59 and L60) carrying the homozygous deletion and the NTC control cell line were treated with $1,25(OH)_2D_3$ or solvent and RT-qPCR assays were performed. The best clone (L60-F6) is shown, while the two remaining are included in Supplementary Figure S11). All expressed genes inside the loop as well as two genes located outside on either side of the loop were studied. (**C**) CRISPR/Cas9-mediated deletion of the right shaded loop anchor and RT-qPCRs were performed as in (B). Two deletion lines obtained from two different gRNA combinations (L66 and L67) were used as whole cell populations after confirming efficient deletion of the anchor region by genomic PCR. The best line (L67) is shown, while L66 is displayed in Supplementary Figure S12. Columns represent the means of three to four independent experiments and the bars indicate standard deviations. Two-tailed Student's *t*-tests were performed to determine the significance of the mRNA induction by $1,25(OH)_2D_3$ in reference to solvent-treated cells and of expression changes compared to the NTC control cells (* $P < 0.05$; ** $P < 0.01$; *** $P < 0.001$).

VDR sites in differential loops supports previous suggestions that TADs also serve to establish a high local transcription factor concentration in the 3D chromatin environment (20). On the other hand, our CRISPRi and anchor deletion results also indicate that the $1,25(OH)_2D_3$-induced dynamic changes of such domains may increase the precision of gene regulation by facilitating enhancer-promoter contacts and by supporting CTCF to maintain TADs and sub-TADs. Globally, the maintenance of 3D chromatin architecture has been shown as non-essential for enhancer-promoter interactions and resulting gene expression. Our results are consistent with a more complex role of genome topology in transcriptional regulation. For vitamin D signaling, we could describe different gene regulatory scenarios, in which CTCF loops are required for a full response of target genes to the stimulation. The term Regulatory Chromatin Domains (RCD) has been proposed for such scenarios (60). Among differential contacts, upregulated loops were overrepresented and enriched for enhancer-promoter interactions. For example, CTCF looping facilitated the contact of a distal VDR enhancer with the TSS of the regulated *PTGES2* gene by dragging the neighboring VDR-bound enhancer along to the TSS of the gene. In addition, CTCF also helps to maintain nucleosome-free regions at both enhancer sites and TSSs (20), thereby facilitating association of VDR to its enhancer and of RNA polymerase II to the TSS. The effects of CRISPRi targeting this VDR co-bound CTCF loop anchor on the vitamin D response were significant, but moderate. This is not surprising, however, considering the presence of multiple additional VDR sites inside the differential loop, which likely contribute to the regulation of the target gene. In other cases, the main function of the differential loops may be to facilitate enhancer-promoter contacts by establishing a short 3D distance, as seen for the *KCNF1* and *ADAM28/ADAMDEC1* loci. The deletion of two different anchors of the three differential loops in the *ADAM28/ADAMDEC1* locus led to similar reductions of the vitamin D response of both target genes, indicating that the three loops do not seem to be functionally redundant, despite the fact that they overlap. In some cases, we have observed an acquired vitamin D responsiveness upon loop anchor deletion for genes located outside of the consequently disrupted loop. Likely, the mechanism underlying this is enhancer hijacking due to a fused domain (20). Future studies will be needed to determine the parameters influencing VDR enhancer-promoter compatibility to be able to predict which genes are likely to be sensitive in that way to the loss of certain insulator sites. An interesting and novel finding of our study is that the dynamic CTCF loop changes upon $1,25(OH)_2D_3$ treatment can not only be related to the presence of VDR in the loop, but also to the binding of VDR-downstream transcription factors in the anchor regions. Thus, adjustments of the chromatin 3D structure provide a mechanism for the fine-regulation of both primary and secondary vitamin D target genes. In a previous study, we have observed that 15% of all VDR ChIP-seq peaks overlapped with CTCF peaks, but there was no indication that VDR and CTCF are part of the same nuclear protein complex (73). Consistently, we found in this study that VDR frequently binds close to differential CTCF loop anchors, but a direct co-location was comparatively rare. Thus, VDR could either influence CTCF binding to DNA by short transient contacts via looping, or by a spreading of VDR-mediated histone acetylation and chromatin opening along the DNA strand. It is also possible that, as described for estrogen (77), also $1,25(OH)_2D_3$ increases CTCF binding to enhancer RNAs, which then facilitate CTCF association to enhancer DNA.

It appears likely that additional mechanisms that have been described for other nuclear receptors also apply to vitamin D signaling, thereby adding another layer of complexity (74,77,103,105). Interaction of nuclear lamina-bound CTCF with VDR enhancers could limit the formation of VDR loops. Functional binding of ligand-bound and ligand-free VDR may be a prerequisite for regulation of enhancer blocking and basal enhancer insulation, respectively. In this respect, it can be hypothesized that boundary RNAs induced by active VDR enhancers may enhance TAD insulation by recruiting or stabilizing CTCF (106). Finally, equivalent to LDECs (ligand-dependent ERα enhancer clusters) (103), VDR may form ligand-dependent VDR enhancer clusters in 3D. The investigation of such mechanisms was outside the scope of this study.

In summary, we could show that activation of the vitamin D receptor with its high affinity ligand $1,25(OH)_2D_3$ induced 3D chromatin changes, which are functionally important for the regulation of primary and secondary vitamin D target genes. Considering that all nuclear receptors follow the same general principle of gene regulation, we hypothesize that the Regulatory Chromatin Domains we have identified for VDR provide a general principle for fine-tuning of gene regulation by all members of the nuclear receptor superfamily.

DATA AVAILABILITY

Unprocessed CTCF HiChIP sequencing data is available at the NCBI Sequence Read Archive (SRA) under the BioProject ID PRJNA750260. Processed loop data including fold changes and differential statistics are available at the NCBI Gene Expression Omnibus (GEO) under the accession GSE188380. Hi-C data is available at GEO under the accession GSE190463.

SUPPLEMENTARY DATA

Supplementary Data are available at NAR Online.

ACKNOWLEDGEMENTS

We thank Tanja Lüneburg for expert technical assistance. Kind thanks to Dr Stefan Günther at Max-Planck-Institute for Heart and Lung Research, Bad Nauheim, Germany, for sequencing of the Hi-C libraries.

FUNDING

Deutsche Forschungsgemeinschaft [437173059 to S.S., SFB1039 TPA01 to R.P.B., EXS2026 'CPI – Cardiopulmonary institute']; DZHK; Goethe University, Frankfurt. Funding for open access charge: Goethe University Frankfurt.

Conflict of interest statement. None declared.

REFERENCES

1. Rao,S.S., Huntley,M.H., Durand,N.C., Stamenova,E.K., Bochkov,I.D., Robinson,J.T., Sanborn,A.L., Machol,I., Omer,A.D., Lander,E.S. *et al.* (2014) A 3D map of the human genome at kilobase resolution reveals principles of chromatin looping. *Cell*, **159**, 1665–1680.
2. Lieberman-Aiden,E., van Berkum,N.L., Williams,L., Imakaev,M., Ragoczy,T., Telling,A., Amit,I., Lajoie,B.R., Sabo,P.J., Dorschner,M.O. *et al.* (2009) Comprehensive mapping of long-range interactions reveals folding principles of the human genome. *Science*, **326**, 289–293.
3. Dixon,J.R., Selvaraj,S., Yue,F., Kim,A., Li,Y., Shen,Y., Hu,M., Liu,J.S. and Ren,B. (2012) Topological domains in mammalian genomes identified by analysis of chromatin interactions. *Nature*, **485**, 376–380.
4. Nora,E.P., Lajoie,B.R., Schulz,E.G., Giorgetti,L., Okamoto,I., Servant,N., Piolot,T., van Berkum,N.L., Meisig,J., Sedat,J. *et al.* (2012) Spatial partitioning of the regulatory landscape of the X-inactivation centre. *Nature*, **485**, 381–385.
5. de Wit,E. (2020) TADs as the caller calls them. *J. Mol. Biol.*, **432**, 638–642.
6. Beagan,J.A. and Phillips-Cremins,J.E. (2020) On the existence and functionality of topologically associating domains. *Nat. Genet.*, **52**, 8–16.
7. Dekker,J. and Mirny,L. (2016) The 3D genome as moderator of chromosomal communication. *Cell*, **164**, 1110–1121.
8. Fudenberg,G., Imakaev,M., Lu,C., Goloborodko,A., Abdennur,N. and Mirny,L.A. (2016) Formation of chromosomal domains by loop extrusion. *Cell Rep.*, **15**, 2038–2049.
9. Nuebler,J., Fudenberg,G., Imakaev,M., Abdennur,N. and Mirny,L.A. (2018) Chromatin organization by an interplay of loop extrusion and compartmental segregation. *Proc. Natl. Acad. Sci. U.S.A.*, **115**, E6697–E6706.
10. Szabo,Q., Donjon,A., Jerković,I., Papadopoulos,G.L., Cheutin,T., Bonev,B., Nora,E.P., Bruneau,B.G., Bantignies,F. and Cavalli,G. (2020) Regulation of single-cell genome organization into TADs and chromatin nanodomains. *Nat. Genet.*, **52**, 1151–1157.
11. Nora,E.P., Goloborodko,A., Valton,A.L., Gibcus,J.H., Uebersohn,A., Abdennur,N., Dekker,J., Mirny,L.A. and Bruneau,B.G. (2017) Targeted degradation of CTCF decouples local insulation of chromosome domains from genomic compartmentalization. *Cell*, **169**, 930–944.
12. Rao,S.S.P., Huang,S.C., Glenn St Hilaire,B., Engreitz,J.M., Perez,E.M., Kieffer-Kwon,K.R., Sanborn,A.L., Johnstone,S.E., Bascom,G.D., Bochkov,I.D. *et al.* (2017) Cohesin loss eliminates all loop domains. *Cell*, **171**, 305–320.
13. Schwarzer,W., Abdennur,N., Goloborodko,A., Pekowska,A., Fudenberg,G., Loe-Mie,Y., Fonseca,N.A., Huber,W., Haering,C.H., Mirny,L. *et al.* (2017) Two independent modes of chromatin organization revealed by cohesin removal. *Nature*, **551**, 51–56.
14. Wutz,G., Varnai,C., Nagasaka,K., Cisneros,D.A., Stocsits,R.R., Tang,W., Schoenfelder,S., Jessberger,G., Muhar,M., Hossain,M.J. *et al.* (2017) Topologically associating domains and chromatin loops depend on cohesin and are regulated by CTCF, WAPL, and PDS5 proteins. *EMBO J.*, **36**, 3573–3599.
15. Fujioka,M., Sun,G. and Jaynes,J.B. (2013) The drosophila eve insulator homie promotes eve expression and protects the adjacent gene from repression by polycomb spreading. *PLoS Genet.*, **9**, e1003883.
16. Narendra,V., Rocha,P.P., An,D., Raviram,R., Skok,J.A., Mazzoni,E.O. and Reinberg,D. (2015) CTCF establishes discrete functional chromatin domains at the hox clusters during differentiation. *Science*, **347**, 1017–1021.
17. Geyer,P.K. and Corces,V.G. (1992) DNA position-specific repression of transcription by a drosophila zinc finger protein. *Genes Dev.*, **6**, 1865–1873.
18. Muravyova,E., Golovnin,A., Gracheva,E., Parshikov,A., Belenkaya,T., Pirrotta,V. and Georgiev,P. (2001) Loss of insulator activity by paired su(hw) chromatin insulators. *Science*, **291**, 495–498.
19. Hou,C., Zhao,H., Tanimoto,K. and Dean,A. (2008) CTCF-dependent enhancer-blocking by alternative chromatin loop formation. *Proc. Natl. Acad. Sci. U.S.A.*, **105**, 20398–20403.
20. Cavalheiro,G.R., Pollex,T. and Furlong,E.E. (2021) To loop or not to loop: what is the role of TADs in enhancer function and gene regulation?*Curr. Opin. Genet. Dev.*, **67**, 119–129.
21. Hansen,A.S., Pustova,I., Cattoglio,C., Tjian,R. and Darzacq,X. (2017) CTCF and cohesin regulate chromatin loop stability with distinct dynamics. *Elife*, **6**, e25776.
22. Despang,A., Schöpflin,R., Franke,M., Ali,S., Jerković,I., Paliou,C., Chan,W.L., Timmermann,B., Wittler,L., Vingron,M. *et al.* (2019) Functional dissection of the sox9-kcnj2 locus identifies nonessential and instructive roles of TAD architecture. *Nat. Genet.*, **51**, 1263–1271.
23. Flavahan,W.A., Drier,Y., Liau,B.B., Gillespie,S.M., Venteicher,A.S., Stemmer-Rachamimov,A.O., Suvà,M.L. and Bernstein,B.E. (2016) Insulator dysfunction and oncogene activation in IDH mutant gliomas. *Nature*, **529**, 110–114.
24. Hanssen,L.L.P., Kassouf,M.T., Oudelaar,A.M., Biggs,D., Preece,C., Downes,D.J., Gosden,M., Sharpe,J.A., Sloane-Stanley,J.A., Hughes,J.R. *et al.* (2017) Tissue-specific CTCF-cohesin-mediated chromatin architecture delimits enhancer interactions and function in vivo. *Nat. Cell Biol.*, **19**, 952–961.
25. Kloetgen,A., Thandapani,P., Ntziachristos,P., Ghebrechristos,Y., Nomikou,S., Lazaris,C., Chen,X., Hu,H., Bakogianni,S., Wang,J. *et al.* (2020) Three-dimensional chromatin landscapes in t cell acute lymphoblastic leukemia. *Nat. Genet.*, **52**, 388–400.
26. Sima,J., Chakraborty,A., Dileep,V., Michalski,M., Klein,K.N., Holcomb,N.P., Turner,J.L., Paulsen,M.T., Rivera-Mulia,J.C., Trevilla-Garcia,C. *et al.* (2019) Identifying cis elements for spatiotemporal control of mammalian DNA replication. *Cell*, **176**, 816–830.
27. Williamson,I., Kane,L., Devenney,P.S., Flyamer,I.M., Anderson,E., Kilanowski,F., Hill,R.E., Bickmore,W.A. and Lettice,L.A. (2019) Developmentally regulated shh expression is robust to TAD perturbations. *Development*, **146**, dev179523.
28. Yang,M., Vesterlund,M., Siavelis,I., Moura-Castro,L.H., Castor,A., Fioretos,T., Jafari,R., Lilljebjörn,H., Odom,D.T., Olsson,L. *et al.* (2019) Proteogenomics and Hi-C reveal transcriptional dysregulation in high hyperdiploid childhood acute lymphoblastic leukemia. *Nat. Commun.*, **10**, 1519.
29. Rodríguez-Carballo,E., Lopez-Delisle,L., Zhan,Y., Fabre,P.J., Beccari,L., El-Idrissi,I., Huynh,T.H.N., Ozadam,H., Dekker,J. and Duboule,D. (2017) The HoxD cluster is a dynamic and resilient TAD boundary controlling the segregation of antagonistic regulatory landscapes. *Genes Dev.*, **31**, 2264–2281.
30. Lupiáñez,D.G., Kraft,K., Heinrich,V., Krawitz,P., Brancati,F., Klopocki,E., Horn,D., Kayserili,H., Opitz,J.M., Laxova,R. *et al.* (2015) Disruptions of topological chromatin domains cause pathogenic rewiring of gene-enhancer interactions. *Cell*, **161**, 1012–1025.
31. Franke,M., Ibrahim,D.M., Andrey,G., Schwarzer,W., Heinrich,V., Schöpflin,R., Kraft,K., Kempfer,R., Jerković,I., Chan,W.L. *et al.* (2016) Formation of new chromatin domains determines pathogenicity of genomic duplications. *Nature*, **538**, 265–269.
32. Northcott,P.A., Lee,C., Zichner,T., Stütz,A.M., Erkek,S., Kawauchi,D., Shih,D.J., Hovestadt,V., Zapatka,M., Sturm,D. *et al.* (2014) Enhancer hijacking activates GFI1 family oncogenes in medulloblastoma. *Nature*, **511**, 428–434.
33. Hnisz,D., Weintraub,A.S., Day,D.S., Valton,A.L., Bak,R.O., Li,C.H., Goldmann,J., Lajoie,B.R., Fan,Z.P., Sigova,A.A. *et al.* (2016) Activation of proto-oncogenes by disruption of chromosome neighborhoods. *Science*, **351**, 1454–1458.
34. Weischenfeldt,J., Dubash,T., Drainas,A.P., Mardin,B.R., Chen,Y., Stütz,A.M., Waszak,S.M., Bosco,G., Halvorsen,A.R., Raeder,B. *et al.* (2017) Pan-cancer analysis of somatic copy-number alterations implicates IRS4 and IGF2 in enhancer hijacking. *Nat. Genet.*, **49**, 65–74.
35. Melo,U.S., Schöpflin,R., Acuna-Hidalgo,R., Mensah,M.A., Fischer-Zirnsak,B., Holtgrewe,M., Klever,M.K., Türkmen,S., Heinrich,V., Pluym,I.D. *et al.* (2020) Hi-C identifies complex genomic rearrangements and TAD-Shuffling in developmental diseases. *Am. J. Hum. Genet.*, **106**, 872–884.
36. Bender,W. and Lucas,M. (2013) The border between the ultrabithorax and abdominal-A regulatory domains in the drosophila bithorax complex. *Genetics*, **193**, 1135–1147.

37. Arzate-Mejía,R.G., Cerecedo-Castillo,Josué, Guerrero,A., Furlan-Magaril,G. and Recillas-Targa,F. (2020) In situ dissection of domain boundaries affect genome topology and gene transcription in drosophila. *Nat. Commun.*, **11**, 894.
38. Ghavi-Helm,Y., Jankowski,A., Meiers,S., Viales,R.R., Korbel,J.O. and Furlong,E.E.M. (2019) Highly rearranged chromosomes reveal uncoupling between genome topology and gene expression. *Nat. Genet.*, **51**, 1272–1282.
39. Northcott,P.A., Buchhalter,I., Morrissy,A.S., Hovestadt,V., Weischenfeldt,J., Ehrenberger,T., Gröbner,S., Segura-Wang,M., Zichner,T., Rudneva,V.A. *et al.* (2017) The whole-genome landscape of medulloblastoma subtypes. *Nature*, **547**, 311–317.
40. Akdemir,K.C., Le,V.T., Chandran,S., Li,Y., Verhaak,R.G., Beroukhim,R., Campbell,P.J., Chin,L., Dixon,J.R. and Futreal,P.A. (2020) Disruption of chromatin folding domains by somatic genomic rearrangements in human cancer. *Nat. Genet.*, **52**, 294–305.
41. ENCODE-Project-Consortium. (2012) An integrated encyclopedia of DNA elements in the human genome. *Nature*, **489**, 57–74.
42. Heidari,N., Phanstiel,D.H., He,C., Grubert,F., Jahanbani,F., Kasowski,M., Zhang,M.Q. and Snyder,M.P. (2014) Genome-wide map of regulatory interactions in the human genome. *Genome Res.*, **24**, 1905–1917.
43. Naumova,N., Imakaev,M., Fudenberg,G., Zhan,Y., Lajoie,B.R., Mirny,L.A. and Dekker,J. (2013) Organization of the mitotic chromosome. *Science*, **342**, 948–953.
44. Cuddapah,S., Jothi,R., Schones,D.E., Roh,T.Y., Cui,K. and Zhao,K. (2009) Global analysis of the insulator binding protein CTCF in chromatin barrier regions reveals demarcation of active and repressive domains. *Genome Res.*, **19**, 24–32.
45. Calero-Nieto,F.J., Ng,F.S., Wilson,N.K., Hannah,R., Moignard,V., Leal-Cervantes,A.I., Jimenez-Madrid,I., Diamanti,E., Wernisch,L. and Gottgens,B. (2014) Key regulators control distinct transcriptional programmes in blood progenitor and mast cells. *EMBO J.*, **33**, 1212–1226.
46. Lee,B.K., Bhinge,A.A., Battenhouse,A., McDaniell,R.M., Liu,Z., Song,L., Ni,Y., Birney,E., Lieb,J.D., Furey,T.S. *et al.* (2012) Cell-type specific and combinatorial usage of diverse transcription factors revealed by genome-wide binding studies in multiple human cells. *Genome Res.*, **22**, 9–24.
47. Shen,Y., Yue,F., McCleary,D.F., Ye,Z., Edsall,L., Kuan,S., Wagner,U., Dixon,J., Lee,L., Lobanenkov,V.V. *et al.* (2012) A map of the cis-regulatory sequences in the mouse genome. *Nature*, **488**, 116–120.
48. Martin,D., Pantoja,C., Fernandez Minan,A., Valdes-Quezada,C., Molto,E., Matesanz,F., Bogdanovic,O., de la Calle-Mustienes,E., Dominguez,O., Taher,L. *et al.* (2011) Genome-wide CTCF distribution in vertebrates defines equivalent sites that aid the identification of disease-associated genes. *Nat. Struct. Mol. Biol.*, **18**, 708–714.
49. Sheffield,N.C., Thurman,R.E., Song,L., Safi,A., Stamatoyannopoulos,J.A., Lenhard,B., Crawford,G.E. and Furey,T.S. (2013) Patterns of regulatory activity across diverse human cell types predict tissue identity, transcription factor binding, and long-range interactions. *Genome Res.*, **23**, 777–788.
50. Schwalie,P.C., Ward,M.C., Cain,C.E., Faure,A.J., Gilad,Y., Odom,D.T. and Flicek,P. (2013) Co-binding by YY1 identifies the transcriptionally active, highly conserved set of CTCF-bound regions in primate genomes. *Genome Biol.*, **14**, R148.
51. Dixon,J.R., Jung,I., Selvaraj,S., Shen,Y., Antosiewicz-Bourget,J.E., Lee,A.Y., Ye,Z., Kim,A., Rajagopal,N., Xie,W. *et al.* (2015) Chromatin architecture reorganization during stem cell differentiation. *Nature*, **518**, 331–336.
52. Criscione,S.W., De Cecco,M., Siranosian,B., Zhang,Y., Kreiling,J.A., Sedivy,J.M. and Neretti,N. (2016) Reorganization of chromosome architecture in replicative cellular senescence. *Sci. Adv.*, **2**, e1500882.
53. Siersbæk,R., Madsen,J.G.S., Javierre,B.M., Nielsen,R., Bagge,E.K., Cairns,J., Wingett,S.W., Traynor,S., Spivakov,M., Fraser,P. *et al.* (2017) Dynamic rewiring of promoter-anchored chromatin loops during adipocyte differentiation. *Mol. Cell*, **66**, 420–435.
54. Ray,J., Munn,P.R., Vihervaara,A., Lewis,J.J., Ozer,A., Danko,C.G. and Lis,J.T. (2019) Chromatin conformation remains stable upon extensive transcriptional changes driven by heat shock. *Proc. Natl. Acad. Sci. U.S.A.*, **116**, 19431–19439.
55. Hyle,J., Zhang,Y., Wright,S., Xu,B., Shao,Y., Easton,J., Tian,L., Feng,R., Xu,P. and Li,C. (2019) Acute depletion of CTCF directly affects MYC regulation through loss of enhancer-promoter looping. *Nucleic Acids Res.*, **47**, 6699–6713.
56. Soshnikova,N., Montavon,T., Leleu,M., Galjart,N. and Duboule,D. (2010) Functional analysis of CTCF during mammalian limb development. *Dev. Cell*, **19**, 819–830.
57. Wan,L.B., Pan,H., Hannenhalli,S., Cheng,Y., Ma,J., Fedoriw,A., Lobanenkov,V., Latham,K.E., Schultz,R.M. and Bartolomei,M.S. (2008) Maternal depletion of CTCF reveals multiple functions during oocyte and preimplantation embryo development. *Development*, **135**, 2729–2738.
58. Zuin,J., Dixon,J.R., van der Reijden,M.I., Ye,Z., Kolovos,P., Brouwer,R.W., van de Corput,M.P., van de Werken,H.J., Knoch,T.A., van,I.W.F. *et al.* (2014) Cohesin and CTCF differentially affect chromatin architecture and gene expression in human cells. *Proc. Nat. Acad. Sci. U.S.A.*, **111**, 996–1001.
59. Splinter,E., Heath,H., Kooren,J., Palstra,R.J., Klous,P., Grosveld,F., Galjart,N. and de Laat,W. (2006) CTCF mediates long-range chromatin looping and local histone modification in the beta-globin locus. *Genes Dev.*, **20**, 2349–2354.
60. Ibrahim,D.M. and Mundlos,S. (2020) The role of 3D chromatin domains in gene regulation: a multi-facetted view on genome organization. *Curr. Opin. Genet. Dev.*, **61**, 1–8.
61. Glass,C.K. and Ogawa,S. (2006) Combinatorial roles of nuclear receptors in inflammation and immunity. *Nat. Rev. Immunol.*, **6**, 44–55.
62. Kininis,M. and Kraus,W.L. (2008) A global view of transcriptional regulation by nuclear receptors: gene expression, factor localization, and DNA sequence analysis. *Nucl. Recept. Signal.*, **6**, e005.
63. Porter,B.A., Ortiz,M.A., Bratslavsky,G. and Kotula,L. (2019) Structure and function of the nuclear receptor superfamily and current targeted therapies of prostate cancer. *Cancers*, **11**, 1852.
64. Carlberg,C. and Dunlop,T.W. (2006) An integrated biological approach to nuclear receptor signaling in physiological control and disease. *Crit. Rev. Eukaryot. Gene Expr.*, **16**, 1–22.
65. Haussler,M.R., Haussler,C.A., Bartik,L., Whitfield,G.K., Hsieh,J.C., Slater,S. and Jurutka,P.W. (2008) Vitamin d receptor: molecular signaling and actions of nutritional ligands in disease prevention. *Nutr. Rev.*, **66**, S98–S112.
66. Pike,J.W., Meyer,M.B., Watanuki,M., Kim,S., Zella,L.A., Fretz,J.A., Yamazaki,M. and Shevde,N.K. (2007) Perspectives on mechanisms of gene regulation by 1,25-dihydroxyvitamin D3 and its receptor. *J. Steroid Biochem. Mol. Biol.*, **103**, 389–395.
67. Seuter,S., Neme,A. and Carlberg,C. (2017) Epigenomic PU.1-VDR crosstalk modulates vitamin d signaling. *Biochim. Biophys. Acta*, **1860**, 405–415.
68. Nurminen,V., Neme,A., Seuter,S. and Carlberg,C. (2019) Modulation of vitamin d signaling by the pioneer factor CEBPA. *Biochim. Biophys. Acta Gene Regul. Mech.*, **1862**, 96–106.
69. Molnár,F. (2014) Structural considerations of vitamin d signaling. *Front. Physiol.*, **5**, 191.
70. Wei,Z., Yoshihara,E., He,N., Hah,N., Fan,W., Pinto,A.F.M., Huddy,T., Wang,Y., Ross,B., Estepa,G. *et al.* (2018) Vitamin d switches BAF complexes to protect β cells. *Cell*, **173**, 1135–1149.
71. Pereira,F., Barbáchano,A., Silva,J., Bonilla,F., Campbell,M.J., Muñoz,A. and Larriba,M.J. (2011) KDM6B/JMJD3 histone demethylase is induced by vitamin d and modulates its effects in colon cancer cells. *Hum. Mol. Genet.*, **20**, 4655–4665.
72. Nurminen,V., Neme,A., Seuter,S. and Carlberg,C. (2018) The impact of the vitamin D-modulated epigenome on VDR target gene regulation. *Biochim. Biophys. Acta Gene Regul. Mech.*, **1861**, 697–705.
73. Seuter,S., Neme,A. and Carlberg,C. (2016) Epigenome-wide effects of vitamin d and their impact on the transcriptome of human monocytes involve CTCF. *Nucleic Acids Res.*, **44**, 4090–4104.
74. Weth,O., Weth,C., Bartkuhn,M., Leers,J., Uhle,F. and Renkawitz,R. (2010) Modular insulators: genome wide search for composite CTCF/thyroid hormone receptor binding sites. *PLoS One*, **5**, e10119.
75. Lutz,M., Burke,L.J., LeFevre,P., Myers,F.A., Thorne,A.W., Crane-Robinson,C., Bonifer,C., Filippova,G.N., Lobanenkov,V. and Renkawitz,R. (2003) Thyroid hormone-regulated enhancer

blocking: cooperation of CTCF and thyroid hormone receptor. *EMBO J.*, **22**, 1579–1587.
76. Ishihara,K., Nakamoto,M. and Nakao,M. (2016) DNA methylation-independent removable insulator controls chromatin remodeling at the HOXA locus via retinoic acid signaling. *Hum. Mol. Genet.*, **25**, 5383–5394.
77. Fiorito,E., Sharma,Y., Gilfillan,S., Wang,S., Singh,S.K., Satheesh,S.V., Katika,M.R., Urbanucci,A., Thiede,B., Mills,I.G. *et al.* (2016) CTCF modulates estrogen receptor function through specific chromatin and nuclear matrix interactions. *Nucleic Acids Res.*, **44**, 10588–10602.
78. Achinger-Kawecka,J., Valdes-Mora,F., Luu,P.L., Giles,K.A., Caldon,C.E., Qu,W., Nair,S., Soto,S., Locke,W.J., Yeo-Teh,N.S. *et al.* (2020) Epigenetic reprogramming at estrogen-receptor binding sites alters 3D chromatin landscape in endocrine-resistant breast cancer. *Nat. Commun.*, **11**, 320.
79. Neme,A., Seuter,S. and Carlberg,C. (2016) Vitamin D-dependent chromatin association of CTCF in human monocytes. *Biochim. Biophys. Acta*, **1859**, 1380–1388.
80. Mumbach,M.R., Rubin,A.J., Flynn,R.A., Dai,C., Khavari,P.A., Greenleaf,W.J. and Chang,H.Y. (2016) HiChIP: efficient and sensitive analysis of protein-directed genome architecture. *Nat. Methods*, **13**, 919–922.
81. Servant,N., Varoquaux,N., Lajoie,B.R., Viara,E., Chen,C.J., Vert,J.P., Heard,E., Dekker,J. and Barillot,E. (2015) HiC-Pro: an optimized and flexible pipeline for Hi-C data processing. *Genome Biol.*, **16**, 259.
82. Lareau,C.A. and Aryee,M.J. (2018) hichipper: a preprocessing pipeline for calling DNA loops from HiChIP data. *Nat. Methods*, **15**, 155–156.
83. Lareau,C.A. and Aryee,M.J. (2018) diffloop: a computational framework for identifying and analyzing differential DNA loops from sequencing data. *Bioinformatics*, **34**, 672–674.
84. Baumgarten,N., Hecker,D., Karunanithi,S., Schmidt,F., List,M. and Schulz,M.H. (2020) EpiRegio: analysis and retrieval of regulatory elements linked to genes. *Nucleic. Acids. Res.*, **48**, W193–W199.
85. Harmston,N., Ing-Simmons,E., Perry,M., Barešić,A. and Lenhard,B. (2015) GenomicInteractions: an R/Bioconductor package for manipulating and investigating chromatin interaction data. *BMC Genomics*, **16**, 963.
86. Quinlan,A.R. and Hall,I.M. (2010) BEDTools: a flexible suite of utilities for comparing genomic features. *Bioinformatics*, **26**, 841–842.
87. van der Weide,R.H., van den Brand,T., Haarhuis,J.H.I., Teunissen,H., Rowland,B.D. and de Wit,E. (2021) Hi-C analyses with GENOVA: a case study with cohesin variants. *NAR Genom. Bioinform.*, **3**, lqab040.
88. Wolff,J., Rabbani,L., Gilsbach,R., Richard,G., Manke,T., Backofen,R. and Grüning,B.A. (2020) Galaxy hicexplorer 3: a web server for reproducible Hi-C, capture Hi-C and single-cell Hi-C data analysis, quality control and visualization. *Nucleic. Acids. Res.*, **48**, W177–W184.
89. Cresswell,K.G. and Dozmorov,M.G. (2020) TADCompare: an r package for differential and temporal analysis of topologically associated domains. *Front. Genet.*, **11**, 158.
90. Schmidt,F., Kern,F., Ebert,P., Baumgarten,N. and Schulz,M.H. (2019) TEPIC 2-an extended framework for transcription factor binding prediction and integrative epigenomic analysis. *Bioinformatics*, **35**, 1608–1609.
91. Fornes,O., Castro-Mondragon,J.A., Khan,A., van der Lee,R., Zhang,X., Richmond,P.A., Modi,B.P., Correard,S., Gheorghe,M., Baranasic,D. *et al.* (2020) JASPAR 2020: update of the open-access database of transcription factor binding profiles. *Nucleic Acids Res.*, **48**, D87–D92.
92. Kulakovskiy,I.V., Vorontsov,I.E., Yevshin,I.S., Sharipov,R.N., Fedorova,A.D., Rumynskiy,E.I., Medvedeva,Y.A., Magana-Mora,A., Bajic,V.B., Papatsenko,D.A. *et al.* (2018) HOCOMOCO: towards a complete collection of transcription factor binding models for human and mouse via large-scale chip-Seq analysis. *Nucleic Acids Res.*, **46**, D252–D259.
93. Kheradpour,P. and Kellis,M. (2014) Systematic discovery and characterization of regulatory motifs in ENCODE TF binding experiments. *Nucleic Acids Res.*, **42**, 2976–2987.
94. Gérard,D., Schmidt,F., Ginolhac,A., Schmitz,M., Halder,R., Ebert,P., Schulz,M.H., Sauter,T. and Sinkkonen,L. (2019) Temporal enhancer profiling of parallel lineages identifies AHR and GLIS1 as regulators of mesenchymal multipotency. *Nucleic Acids Res.*, **47**, 1141–1163.
95. Engler,C., Kandzia,R. and Marillonnet,S. (2008) A one pot, one step, precision cloning method with high throughput capability. *PLoS One*, **3**, e3647.
96. Sanjana,N.E., Shalem,O. and Zhang,F. (2014) Improved vectors and genome-wide libraries for CRISPR screening. *Nat. Methods*, **11**, 783–784.
97. Thakore,P.I., D'Ippolito,A.M., Song,L., Safi,A., Shivakumar,N.K., Kabadi,A.M., Reddy,T.E., Crawford,G.E. and Gersbach,C.A. (2015) Highly specific epigenome editing by CRISPR-Cas9 repressors for silencing of distal regulatory elements. *Nat. Methods*, **12**, 1143–1149.
98. Seuter,S., Heikkinen,S. and Carlberg,C. (2013) Chromatin acetylation at transcription start sites and vitamin d receptor binding regions relates to effects of 1alpha,25-dihydroxyvitamin D3 and histone deacetylase inhibitors on gene expression. *Nucleic Acids Res.*, **41**, 110–124.
99. Neme,A., Seuter,S. and Carlberg,C. (2017) Selective regulation of biological processes by vitamin d based on the spatio-temporal cistrome of its receptor. *Biochim. Biophys. Acta*, **1860**, 952–961.
100. Warwick,T., Schulz,M.H., Günther,S., Gilsbach,R., Neme,A., Carlberg,C., Brandes,R.P. and Seuter,S. (2021) A hierarchical regulatory network analysis of the vitamin d induced transcriptome reveals novel regulators and complete VDR dependency in monocytes. *Sci. Rep.*, **11**, 6518.
101. Lin,D., Hong,P., Zhang,S., Xu,W., Jamal,M., Yan,K., Lei,Y., Li,L., Ruan,Y., Fu,Z.F. *et al.* (2018) Digestion-ligation-only Hi-C is an efficient and cost-effective method for chromosome conformation capture. *Nat. Genet.*, **50**, 754–763.
102. Robinson,J.T., Thorvaldsdóttir,H., Winckler,W., Guttman,M., Lander,E.S., Getz,G. and Mesirov,J.P. (2011) Integrative genomics viewer. *Nat. Biotechnol.*, **29**, 24–26.
103. Saravanan,B., Soota,D., Islam,Z., Majumdar,S., Mann,R., Meel,S., Farooq,U., Walavalkar,K., Gayen,S., Singh,A.K. *et al.* (2020) Ligand dependent gene regulation by transient ERα clustered enhancers. *PLoS Genet.*, **16**, e1008516.
104. Fleet,J.C., Aldea,D., Chen,L., Christakos,S. and Verzi,M. (2022) Regulatory domains controlling high intestinal vitamin d receptor (VDR) gene expression are conserved in mouse and human. *J. Biol. Chem.*, 101616.
105. Fullwood,M.J., Liu,M.H., Pan,Y.F., Liu,J., Xu,H., Mohamed,Y.B., Orlov,Y.L., Velkov,S., Ho,A., Mei,P.H. *et al.* (2009) An oestrogen-receptor-alpha-bound human chromatin interactome. *Nature*, **462**, 58–64.
106. Islam,Z., Saravanan,B., Walavalkar,K., Farooq,U., Kumar Singh,A., Thakur,J., Pandit,A., Sabarinathan,R., Henikoff,S. and Notani,D. (2021) Active enhancers strengthen TAD insulation by bRNA mediated CTCF enrichment at the TAD boundaries. bioRxiv doi: https://doi.org/10.1101/2021.07.13.452118, 16 July 2021, preprint: not peer reviewed.